Australian Government
Department of Defence
Defence Science and
Technology Organisation

A Model of Low Grazing Angle Sea Clutter for Coherent Radar Performance Analysis

J L Whitrow

Electronic Warfare and Radar Division

Defence Science and Technology Organisation

DSTO–TR–2864

ABSTRACT

Pulse Doppler radar systems are increasingly being used for airborne maritime surveillance roles, but current models for sea clutter do not incorporate the spectral information required to analyse the detection performance of these systems in the low grazing angle maritime environment. This report uses standard radar sea clutter models, and spectral information from wavetank and open ocean measurements to deduce the amplitudes, Doppler frequencies, and bandwidths of the Bragg, whitecap and spike components, which together comprise the sea clutter return. This version of the report incorporates corrections listed in the Corrigenda.

APPROVED FOR PUBLIC RELEASE

Published by

DSTO Defence Science and Technology Organisation
PO Box 1500
Edinburgh, South Australia 5111, Australia

Telephone: (08) 7389 5555
Facsimile: (08) 7389 6567

AR No. 015-661
June, 2013
Corrected March, 2017

APPROVED FOR PUBLIC RELEASE

A Model of Low Grazing Angle Sea Clutter for Coherent Radar Performance Analysis

Executive Summary

Airborne pulse Doppler radar systems developed for air-to-air applications are increasingly being used in the maritime surveillance role. Because of the relatively low peak powers of these radars compared with dedicated maritime surveillance radars, they tend to use coherent processing to enhance the signal-to-clutter-plus-noise ratio sufficiently for target detection. In analysing the performance of these radars, conventional low grazing angle models for the sea clutter are inadequate as they provide only the mean radar cross section for horizontal and vertical polarisation. To correctly estimate coherent radar performance, the Doppler characteristics of sea clutter are required, but there are no models describing this aspect of sea clutter in the open literature. This work seeks to develop a suitable Doppler model from conventional clutter models based on information on the Doppler characteristics of sea clutter from wavetank and ocean data collection.

Three conventional clutter models, namely the GIT, Hybrid and NRL models, which provide estimates of the mean radar cross section for horizontal and vertical polarisation as a function of radar frequency, sea state, grazing angle, and wind aspect angle, are documented. They are then modified to comply with recently published measurements of the variation of vertical polarisation clutter with aspect angle which differs from the original data used to develop these models. We then review research on the spectral characteristics of waves, which shows that sea clutter can be described by three separate components, Bragg scattering, whitecap scattering and spike scattering, each with a characteristic Doppler peak frequency and spectral bandwidth. Then, based on assumptions of the relative amplitudes of these components as a function of wind speed, and the peak frequencies and bandwidths obtained from wavetank data, we describe two methods for deducing the amplitudes of the spectral components from the conventional clutter models.

Charts are provided of the Bragg, whitecap and spike terms for both horizontal and vertical polarisations as a function of wind aspect angle for sea states 1 to 5, determined by the two methods, for each of the conventional clutter models. There is considerable similarity of form between the clutter models, the differences mainly resulting from the different clutter levels predicted by the models. Which clutter model is selected may depend upon the requirements of the study for which the spectrum is required. The two methods have slightly different variations as a function of wind aspect, but it is not possible from current sea clutter data to select one as being preferred. There is little difference in the overall spectra from the three clutter models, and only that obtained from the NRL model are presented in this report. A comparison of the results with the limited published open ocean spectra data indicates that the model described will be a useful tool.

THIS PAGE IS INTENTIONALLY BLANK

Author

John L Whitrow
Electronic Warfare and Radar Division

John Whitrow joined the then WRE as a Cadet, Defence Science in 1963, while studying for a combined science and electrical engineering degree at the University of Adelaide. Upon graduation, he was appointed as a Scientific Officer in Electronic Techniques Group where he worked on electromagnetic theory, antennas and microwave components. Between 1971 and 1974 he carried out research for a Ph.D. in diffraction theory at Monash University, continuing in the same line of research on return to Edinburgh. In 1979 he was promoted to SRS to work on the analysis of microwave radar system performance. In this period, he also represented the Department of Defence in the development of Australian Standard AS-2772 covering exposure of personnel to microwave radiation. In 1990 he became a Group Head, continuing to work on microwave radar systems. During his career, he has been involved in providing radar system advice on a number of major acquisition projects. Currently his primary interest is the analysis of performance of airborne pulse Doppler radar systems, for both air-to-air and air-to-sea-surface applications.

THIS PAGE IS INTENTIONALLY BLANK

Contents

THIS PAGE IS INTENTIONALLY BLANK

Corrigenda

1. page 5, equation 13, second line, changed exponent of $H_{\text{av}} + 0.015$ from -0.24 to -0.4.
2. page 5, equation 13, both lines, changed $\psi + 0.001$ to $\psi + 0.0001$.

THIS PAGE IS INTENTIONALLY BLANK

1 Introduction

Sea clutter has been studied extensively since the development of airborne maritime surveillance and naval radars in World War 2. In the version of the radar equation for estimating performance of these radars [7], the effect of sea clutter is included as a simple term σ_0, the radar cross section per unit area of the ocean surface, which is then multiplied by the effective area of the radar resolution cell to provide the total clutter signal against which the target signal has to be detected. What is not apparent in the radar equation is that this term is dependent on a large number of physical parameters of the ocean environment, the wind strength, the duration of the wind, and the fetch (usually these three parameters are combined as a sea state term), the wind direction relative to the radar look direction, the grazing angle of the radar beam with respect to the surface, and the presence of swell. There are also radar system parameters which can impact the observed value of σ_0, the radar frequency, the pulse repetition frequency, the antenna polarisation, and the resolution cell size. Propagation conditions in the atmosphere, especially ducting, also influence the observed clutter cross section. Nathanson in his second edition of *Radar Design Principles* [7] cites no fewer than 60 separate clutter measurement studies in developing a set of tables of the mean value of σ_0 as a function of sea state, carrier frequency, polarisation and grazing angle. Usually the radar analyst requires clutter cross section data under conditions differing from that of the measured data, and consequently a number of formulas have been developed from Nathanson's and other data that approximate the functional form for the average radar cross section of the sea. Notable among these are the Georgia Institute of Technology model (GIT) [6], the Technology Service Corporation model (TSC) [25], and a Hybrid model [21]. The US Naval Research Laboratory [5] and the UK DERA [3] have also developed models for their own applications.

For a number of reasons, coherent pulse Doppler radars developed for air-to-air applications are increasingly being used for maritime surveillance as a secondary role, and these radars tend to have lower peak powers than dedicated airborne maritime surveillance radars. In current designs, they also tend to have longer processed pulse lengths, measured in tenths of microseconds rather than tens of nanoseconds. Recourse to K distribution[1] analysis (see for example Ward, Baker and Watts [28], [1], [29]) or similar is generally not required as conventional Gaussian statistics are adequate to describe the clutter amplitude. These radars rely upon coherent processing to improve the signal-to-clutter-plus-noise ratio sufficiently for target detection, and thus information on the Doppler characteristics of the sea clutter is required for system design and performance estimation. Models to describe the effects of low grazing angle sea clutter on pulse Doppler radar system performance over the range of parameters of operational interest currently do not exist in the open literature.

Observations of sea clutter phenomena, from wavetank experiments and direct measurement of the ocean returns, conclude that there are three separate scattering mechanisms that need to be included in the description of the Doppler characteristics of sea clutter. These mechanisms are resonant Bragg scattering by capillary waves which are modulated by the longer gravity wave structure, scattering by very rough whitecaps produced by breaking waves, and specular reflection from the crest of the wave just before

[1] K is the modified Bessel function of the first kind

it breaks, producing sea spikes [26], [8]. Both amplitude and Doppler characteristics of the scattering mechanisms are required. The relative significance of these phenomena depends upon the incident polarisation. For vertical polarisation, the Bragg scattering term is dominant, whereas with horizontal polarisation this term is only weakly backscattered. Scattering by whitecaps appears to be essentially polarisation independent, whereas the sea spike mechanism produces a much stronger horizontal polarisation response and is virtually absent with vertical polarisation. There is controversy in the literature over whether Bragg scattering occurs at microwave frequencies, see for example articles by Skolnik [24] and Wetzel [31]. The US Naval Research Laboratory has observed that at very high resolution, all clutter appears spiky even at low sea states, and that there is not the continuum of echo signals suggested of Bragg scattering models. However the majority of papers on spectral characteristics of sea clutter refer to Bragg scattering as being the contributor of one component of the clutter, often the most significant, and we shall continue with this terminology as the origin of this signal is not important in this study.

In this report we develop a technique for determining the amplitude and Doppler characteristics of the differing components, in which the spectral parameters of peak frequency and bandwidth are obtained from wavetank measurements of the Doppler characteristics of waves, and then the relative amplitudes of the spectral components are deduced from standard models for σ_0. Comparison are made of the predictions obtained with the GIT, Hybrid and NRL clutter models. We find that the spectrum of open ocean waves is wider than that observed in wavetanks, and the wavetank models need to be multiplied by a scale factor to agree with measurements of ocean waves. Although the emphasis in this report is on the development of the clutter spectral model, it is only a means to an end; to determine the probability of detection of a target in sea clutter when using coherent processing, knowledge is required of the clutter covariance matrix, with which the improvement in signal-to-clutter-plus-noise ratio as a result of the coherent processing can be determined. Farina et. al. [4] have described a technique for determining this improvement factor for a clutter model developed by Lee et. al. [10], and it is simple to adapt to the spectral clutter model that is developed in this report. On the supposition that the Doppler components are statistically independent, it is relatively straightforward to calculate the clutter improvement factor using this method.

Plant and others have published a number of papers in the literature to indicate that a theoretical investigation of the spectra for vertical polarisation sea clutter could be a profitable avenue of investigation, but such an investigation was not considered likely to be completed in time for the particular requirement for which this clutter model was required. Plant et al. [19] extended a composite scattering model down to grazing angles of 1° by incorporating shadowing by the waves into the clutter calculations, and showed that $\sigma_0(VV)$ is explained by the model over the whole range of grazing angles to zenith, but measured $\sigma_0(HH)$ tends to be greater than the model predicts for grazing angles less than about 45°. In an earlier paper, Plant[15] discussed the problem of modelling of Doppler effects in a one dimensional wave, and showed that it is possible to qualitatively predict the observed effects of the Doppler spectra of $\sigma_0\,(HH)$ and $\sigma_0\,(VV)$. However he did not pursue this matter further in his subsequent papers.

In the literature on sea scatter, the angle of the radar beam to the ocean surface is described by either an incidence angle or a grazing angle, the former being more commonly used in the remote sensing literature. The incidence angle refers to the angle the radar

beam propagation direction makes with the normal to the ocean surface, whereas the grazing angle is the angle of the beam to the (tangential) plane of the ocean surface. We will use the latter in this report.

In the documents referenced in this report there is no uniformity in the use of symbols for the input parameters to the models, the sea state, the wind speed and various wave parameters, the grazing angle, and the wind aspect, so where necessary the notation has been changed from the original documentation to ensure consistency within this report. In addition, the values of numerical constants have been changed from the original references so that across all the models, within formulas distances are expressed in metres, velocities in metres/second, and angles in radians.

2 Amplitude Characteristics of Sea Clutter

Most of the early work on sea clutter concentrates on the amplitude characteristics of the clutter, and several differing models to describe the average radar cross section of sea clutter have been developed. The ones that are included in this study are the GIT, Hybrid and NRL models. Our interest is in fully developed seas, primarily sea states 1 to 5, in which it is assumed that the appropriate wind strength has been blowing for the required duration, and that the fetch is sufficient for the seas to fully develop. The sea state, specifically the Douglas sea state, is an integer between 0 and 9, each of which describes a range of sea (and by implication wind) conditions. Within the clutter models though, sea state is treated as a continuous parameter, from which a wind velocity is determined via the formula

$$V_w = 3.16\,\mathrm{SS}^{0.8} \tag{1}$$

Table 1 compares the wind range for each sea state with the wind velocity used in the models, and it can be seen that the models calculate the clutter in the upper portion of the range described by each sea state index.

Table 1: *Comparison of Douglas sea state wind ranges with sea state algorithm*

Sea state	wave height (m)	wind range (m/s)	model wind (m/s)
1	0-0.1	0-3.6	3.2
2	0.1-0.5	3.6-6.2	5.5
3	0.5-1.25	6.2-8.2	7.6
4	1.25-2.5	8.2-9.8	9.6
5	2.5-4.0	9.8-11.8	11.5

For a fully developed sea, there is a simple relationship between the wind speed and the parameters which describe the sea surface. In the GIT model the following relationships are used

$$h_{\mathrm{av}} = 0.08\,\mathrm{SS}^2, \tag{2}$$

and

$$V_w = 8.67\,h_{\mathrm{av}}^{0.4} \tag{3}$$

where h_{av} is the average wave height in metres, SS is the sea state, and V_w is the velocity of the wind in metres/second. The Hybrid model also uses

$$h_{\mathrm{RMS}} = 0.031\,\mathrm{SS}^2 \tag{4}$$

where h_{RMS} is the RMS wave height. In describing sea conditions, the significant wave height, $h_{1/3}$, the average height of the one third highest waves, is the primary indicator of surface roughness, and the NRL model uses the relationship

$$h_{1/3} = 0.049\,\mathrm{SS}^{2.6} \tag{5}$$

though it does not appear directly in their equations. Pidgeon [14] lists a number of other relationships of the "average" wave parameters for a given wind velocity which are useful but are not of significance for the research in this report.

2.1 The GIT Sea Clutter Model

The Georgia Institute of Technology empirical sea clutter model [6] has widespread acceptance as an appropriate model for the mean radar cross section at microwave frequencies at low grazing angle when there is no anomalous propagation. It originally contained two separate expansions covering the frequency ranges 1 to 10 GHz, and 10 to 100 GHz, but subsequently the break point was changed to 12 GHz to include all of X band in the former. The basis of the model is that at low grazing angles, theoretical considerations, supported by observations obtained in non-ducting conditions, indicate that σ_0 varies as the fourth power of the grazing angle, ψ, and above a critical angle flattens off in a plateau region, before increasing rapidly with angles near zenith. Observations culled to retain only non-ducting conditions, were then used to evaluate the parameters in the model. We are concerned with only the lower frequency range expansion in this study.

The GIT model comprises three separate terms, a sea state term, A_w, a multipath term, A_i, and a sea direction term, A_u, each of which are functions of several variables. Data used in the development of the model indicated that the sea state term is more a function of wind speed V_w, than wave height. Plotting σ_0 against the logarithm of the wind speed provided approximately straight lines of the form $(\lambda + 0.015)^{-0.4}$ for low wind speeds, where λ is the radar wavelength (in metres). Taking account of the saturation effect at high speeds, the wind speed factor became

$$A_w = \left[\frac{1.94\,V_w}{1 + V_w/15.4}\right]^{1.1\,(\lambda+0.015)^{-0.4}} \tag{6}$$

For a fully developed sea, wind speed and the average height of the sea are interrelated by

$$V_w = 8.67\,{h_{\mathrm{av}}}^{0.4} \tag{7}$$

where V_w is in meters per second and h_{av} is in metres.

The multipath term is based on interference between a direct ray and a (ocean) surface reflected ray, the amplitude of which is modified by the surface roughness. A surface reflection coefficient of -1 was assumed for all grazing angles, though this is strictly only

accurate for horizontal polarisation. Scattering from a Gaussian surface suggests that the roughness coefficient should be

$$\sigma_\psi = \frac{2\sqrt{2\pi}\ \psi\ h_{\rm av}}{\lambda} \tag{8}$$

where ψ is the grazing angle, and $h_{\rm av}$ is the average wave height. However, Horst et al. observed from experimental data that the roughness parameter is wavelength dependent and they modified Equation 8 to read

$$\sigma_\psi = \frac{(14.4\lambda + 5.5)\ \psi\ h_{\rm av}}{\lambda} \tag{9}$$

It is assumed that ψ is sufficiently small that $\sin\psi \approx \psi$. The interference term then becomes

$$A_i = \frac{{\sigma_\psi}^4}{1 + {\sigma_\psi}^4} \tag{10}$$

The sea direction term is based on upwind-downwind ratio data, and is dependent on the grazing angle , increasing for decreasing grazing angle. The dependence on wind aspect ϕ was based on the observation that σ_0 for HH polarisation in the crosswind direction is about midway in decibel value between the upwind and downwind values. As there was no data to define the functional dependence, a sinusoidal function was chosen,

$$A_u = \exp[\,0.2\,\cos\phi\,(1 - 2.8\,\psi)(\lambda + 0.015)^{-0.4}] \tag{11}$$

for both polarisations, where ϕ is the angle between the radar look direction and the wind direction, having the value 0° when the radar is looking upwind.

The average cross section per unit area of the ocean surface for horizontal polarisation transmission and reception, σ_0^{HH}, is then

$$\sigma_0^{HH} = 3.9 \times 10^{-6}\,\lambda\,\psi^{0.4} A_i\,A_u\,A_w \tag{12}$$

in which the constant term has been experimentally determined, λ is a residual wavelength dependency, and $\psi^{0.4}$ accounts for the effects of shadowing at low angles. The vertical polarisation cross section, σ_0^{VV}, differs from σ_0^{HH} by a multiplicative factor, the form of which depends whether the radar frequency, $f_{\rm RF}$, is greater or less than 3 GHz.[2]

$$\sigma_0^{VV} = \begin{cases} 9.33\,(H_{\rm av} + 0.015)^{-0.24}\,\lambda^{0.25}\,(\psi + 0.0001)^{0.29}\,\sigma_0^{HH} & f_{\rm RF} \geq 3\ \text{GHz} \\ 166.0\,(H_{\rm av} + 0.015)^{-0.4}\,\lambda^{0.87}\,(\psi + 0.0001)^{0.57}\,\sigma_0^{HH} & f_{\rm RF} < 3\ \text{GHz} \end{cases} \tag{13}$$

2.2 Hybrid Sea Clutter Model

The Hybrid sea clutter model was first described in a limited release NATO AAW clutter working group document prepared by J.P.Reilly [20] of Applied Physics Laboratory, Johns Hopkins University. It was intended to provide sea clutter estimates under specific

[2]The formulas for σ_0^{VV} in [6] are written in the form of two expressions for decibels to be subtracted from σ_0^{HH} in dB. These are converted in the above equations to multiplicative terms in linear units for implementation in computer software.

evaporation duct propagation conditions, but at the time of release the propagation study was incomplete. The model was based on published empirical fits to clutter data that included some ducting, including data from Barton [2] and Nathanson [7], and incorporated features of the GIT model. The frequency range of the data base used was from 0.5 to 35 GHz. Subsequently Reilly and Dockery [21] showed that a significant source of variability in sea clutter measurements at low grazing angles can be attributed to variations in the atmospheric refractive index changing propagation conditions near the ocean surface. Accounting for duct induced changes in grazing angle, and in space propagation factor, the output of the GIT model was significantly increased and produced results closer to the Hybrid model.

The Hybrid model is expressed in dB and has the form

$$\sigma_0{}^{\mathrm{dB}} = \sigma_0(\mathrm{ref}) + K_g + K_s + K_p + K_d \tag{14}$$

in which $\sigma_0(\mathrm{ref})$ is a reference reflectivity applying to sea state 5, grazing angle 0.1°, look direction upwind, and vertical polarisation. K_g, K_s, K_p, and K_d are adjustment factors, to accommodate changes from the reference reflectivity in grazing angle, sea state, polarisation and wind direction. The reference reflectivity is

$$\sigma_0(\mathrm{ref}) = \begin{cases} 22.4 \log f_{\mathrm{RF}} - 266.8 & f_{\mathrm{RF}} \le 12.5 \text{ GHz} \\ 3.25 \log f_{\mathrm{RF}} - 71.25 & f_{\mathrm{RF}} > 12.5 \text{ GHz} \end{cases} \tag{15}$$

where f_{RF} is the radar frequency in Hertz.

The adjustment factors are

1. K_g is an adjustment for changes in grazing angle ψ. The reference grazing angle is

$$\psi_r = 0.1^\circ \tag{16}$$

and the transition angle[3] is

$$\psi_t = \sin^{-1}(0.066\,\lambda/h_{\mathrm{RMS}}) \tag{17}$$

where h_{RMS} is the RMS wave height. Then

(a) for $\psi_t \ge \psi_r$

$$K_g = \begin{cases} 0 & \text{for } \psi < \psi_r \\ 20\ \log \psi/\psi_r & \text{for } \psi_r \le \psi \le \psi_t \\ 20\ \log \psi_t/\psi_r + 10\ \log \psi/\psi_t & \text{for } \psi_t \le \psi < 30^\circ \end{cases} \tag{18}$$

(b) for $\psi_t < \psi_r$

$$K_g = \begin{cases} 0 & \text{for } \psi \le \psi_r \\ 10 \log \psi/\psi_r & \text{for } \psi > \psi_r \end{cases} \tag{19}$$

[3] In [21], the numerical factor in the formula is 0.66, which is in error.

2. The sea state adjustment used by Reilly is

$$K_s = 5\,(\mathrm{SS} - 5) \tag{20}$$

which places the lines of integer sea-state at 5 dB intervals at $\psi = 0.1°$, but because the transition angle increases with decreasing sea-state, the curves for sea-states 1 and 2 touch for horizontal polarisation and cross for vertical polarisation, which is clearly not correct. To counter this problem, K_s has been modified in this work to separate out the curves at low sea-state as follows[4]

$$K_s = 5\,(\mathrm{SS} - 5) + \frac{(\mathrm{SS} - 5)^3}{10} \tag{21}$$

with minimal effect at high sea-state.

3. The polarisation adjustment, K_p, is zero for vertical polarisation. For horizontal polarisation it is based on the GIT model[5] and has the value

$$K_p = \begin{cases} 1.7\ln(h_{\mathrm{av}} + 0.015) - 3.8\ln\lambda & \\ \qquad - 2.5\ln(\psi + 0.0001) - 22.2 & f_{\mathrm{RF}} < 3 \text{ GHz} \\ 1.1\ln(h_{\mathrm{av}} + 0.015) - 1.1\lambda & \\ \qquad - 1.3\ln(\psi + 0.0001) - 9.7 & 3 \text{ GHz} \le f_{\mathrm{RF}} \le 10 \text{ GHz} \\ 1.4\ln(h_{\mathrm{av}}) - 3.4\ln\lambda - 1.3\ln\psi - 18.6 & f_{\mathrm{RF}} \ge 10 \text{ GHz} \end{cases} \tag{22}$$

4. The wind direction adjustment K_d is

$$K_d = \left(2 + 1.7\log\frac{0.1}{\lambda}\right)(\cos\phi - 1) \tag{23}$$

where ϕ is the angle between the wind direction and the radar look direction, set to $0°$ when the radar is looking upwind.

The supplementary equations relating wind velocity, RMS wave height and average wave height to sea state used in this model are

$$V_w = 3.2\,\mathrm{SS}^{0.8} \tag{24}$$

$$h_{\mathrm{RMS}} = 0.031\,\mathrm{SS}^2 \tag{25}$$

$$h_{\mathrm{av}} = 0.08\,\mathrm{SS}^2 \tag{26}$$

2.3 The NRL Sea Clutter Model

Gregers-Hansen and Mital [5] have criticised the large average error of both the GIT and Hybrid models when compared with Nathanson's data. In particular they note that the GIT model considerably underestimates the clutter levels at low sea-states. They

[4] In [20] Reilly remarks in the Commentary and Cautionary Notes that the approximation of 5 dB per sea state is excessive for sea states above 6, and understated for sea states below 3.

[5] Note that all the numerical factors have been rounded down from the GIT model

have developed an empirical model seeking to minimise the absolute average error in dB from Nathanson's data, separately optimising the parameters for horizontal and vertical polarisation, of the form

$$\sigma_0{}^{\mathrm{dB}} = c_1 + c_2 \log(\sin\psi) + \frac{(c_3 + c_4\,\psi)\log f_{\mathrm{RF}}}{1 + c_5\,\psi + C_6\,\mathrm{SS}} + c_7(1+\mathrm{SS})^{\frac{1}{2+c_8\,\alpha+c_9\,\mathrm{SS}}} \qquad (27)$$

where f_{RF} is the radar frequency in GHz, and ψ is the grazing angle in radians[6]. One of the claimed advantages of this model is that it includes both sea states 0 and 6. Note, however, that this model provides only the upwind radar cross section, which has the greatest reflectivity of all wind aspects. The parameters of Equation 27 are listed in Table 2.

Table 2: *Parameters for the NRL clutter model*

	Polarisation	
Parameter	Horizontal	Vertical
c_1	-72.76	-48.56
c_2	21.11	26.30
c_3	24.78	29.05
c_4	281.7	-29.70
c_5	35.62	60.56
c_6	-0.02949	0.04839
c_7	26.19	21.37
c_8	5.354	4.278
c_9	0.05031	0.04623

Gregers-Hansen and Mital provided a table comparing the average absolute errors of the GIT, Hybrid, and their model when compared with Nathanson's data, and is reproduced below

Table 3: *RMS errors of clutter models with Nathanson's data*

	Polarisation	
Model	Horizontal	Vertical
GIT	13.7 dB	14.1 dB
Hybrid	14.5 dB	8.7 dB
NRL	2.1 dB	2.0 dB

2.4 Revision of Angular Dependence of Scattering

In the GIT sea clutter model, the aspect dependence is based on upwind-downwind ratio data which was a function of the incidence angle, increasing as the angle decreases, and

[6]In the original paper ψ was expressed in degrees, but in the parameter table the constants c_4, c_5 and c_8 have been multiplied by $180/\pi$ so that it can be expressed in radians.

proportional to $\lambda^{-0.4}$ at $\psi = 0$. For HH polarisation, the crosswind RCS was observed to be about midway in dB between the upwind and downwind RCS, and a simple cosine function was chosen for the angular dependence. This same model was assumed appropriate for VV polarisation. Converting Equation 11 to dB this angular dependence becomes

$$A_u{}^{\mathrm{dB}} = 0.8686 \cos\phi\,(1 - 2.8\,\psi)(\lambda + 0.015)^{-0.4} \tag{28}$$

Note that there is no dependence on the sea state in this expression. In the Hybrid model, the angular dependence in dB is given by Equation 23, and is independent of both sea state and grazing angle, though it is modified by the wavelength.

At high grazing angles both HH and VV polarisation exhibit a different angular behaviour. The RCS exhibits a local maximum at both upwind and downwind look directions, upwind being the greater, with minima in the crosswind directions, i.e. there is a second harmonic dependence of the RCS on the aspect angle. As the grazing angle is reduced, there is point, above 10°, at which the angular behaviour of horizontal polarisation changes to the fundamental, as used in the GIT model. However, in a series of measurements in the South China Sea in 2005, and off the New Jersey USA coast in 2006 Plant et al. [16] found that at low grazing angle, vertical polarisation scatter has a second harmonic dependence and thus is at variance with the GIT model.

Plant published a chart of vertical polarisation measurements at 1° grazing angle and a wavelength of 0.03 m, for wind speeds of 4, 6, and 8 m/s, to each of which we have fitted a three term cosine series. In this data, the variation in cross section with aspect increases with increasing wind velocity. However, these curves have been averaged to provide a result independent of wind velocity to comply with the precepts of the GIT model; the average is

$$A_u^V{}^{\mathrm{dB}} = 1.67 \cos\phi + 3.15 \cos(2\,\phi) \tag{29}$$

If the dependence of the GIT model on ψ and λ is retained, but we otherwise comply with Plant's measurements, then a revised angular dependence model for VV polarisation takes the form

$$A_u^V = \exp\left[(0.2206 \cos(2\,\phi) + 0.1171 \cos\phi)\,(1 - 2.8\psi)\,(\lambda + 0.015)^{-0.4}\right] \tag{30}$$

Plant also provides measurements of the Doppler shifts of vertical polarisation corrected to line of sight velocities, which have a cosinusoidal dependence[7].

Plant's measurements of horizontal polarisation at a grazing angle of 1.7°, and $\lambda =$ 0.03 m suggest that the angular dependence should be

$$A_u^H = 4.43 \cos\phi \tag{31}$$

Thus the revised model for A_u^H in the GIT model becomes

$$A_u^H = \exp\left[0.3219 \cos\phi\,(1 - 2.8\psi)\,(\lambda + 0.015)^{-0.4}\right] \tag{32}$$

In the Hybrid model, the aspect dependency factor is

$$K_d = (0.3 - 1.7 \log\lambda)(\cos\phi - 1) \tag{33}$$

[7]Lamont-Smith [9] did not obtain cosinusoidal dependence for vertical polarisation in his measurements from Portland Bill, only for horizontal polarisation.

which has an average value $-(0.3 - 1.7 \log \lambda)$ at $\phi = \pi/2$. If we scale Plant's result for vertical polarisation according to the dependence of K_d on the radar wavelength, then we have the result

$$K_d^V = (0.3 - 1.7 \log \lambda)(0.578 \cos \phi + 1.09 \cos(2\,\phi) - 1.0) \tag{34}$$

The result for horizontal polarisation is

$$K_d^H = (0.3 - 1.7 \log \lambda)(1.54 \cos \phi - 1.0) \tag{35}$$

Note that the variation in amplitude of horizontal polarisation using Plant's measurements is somewhat greater than in the original Hybrid model.

The NRL model does not include the effect of the wind aspect on the radar cross section, and does not include guidance on how the other parameters affect the aspect dependency. In the absence of any other information we shall assume a functional form identical to that used with the Hybrid model.

Figures 1 and 2 show the horizontal and vertical polarisation predictions of the revised models as a function of the grazing angle for sea states 1 through 5 when looking upwind at a frequency of 9300 MHZ. The GIT and NRL models are comparable at high sea states and large grazing angles, but at low grazing angles especially for sea state 3 and lower, the predictions of the GIT model fall away much more rapidly than those of the NRL model. The Hybrid model gives considerably greater predictions than the other two at high grazing angles for all sea states. In its original form, the separation between curves at low sea states is in error as the curves for sea states 1 and 2 touch for horizontal polarisation and cross in vertical polarisation.

Figure 3 shows the horizontal and vertical polarisation predictions as a function of wind aspect at a grazing angle of 2° for the GIT model. The charts for the angular dependency of the Hybrid and NRL models are similar, the variations in magnitude are the same, the only difference being that the spacing of the sea-state lines corresponds to the different values for the mean radar cross section predicted by these models.

3 Doppler Characteristics of Sea Clutter

Notwithstanding that most maritime radars in the 1950s and 1960s used incoherent processing, during this period there were several investigations of the Doppler characteristics of sea clutter. The most significant of these was that of Pidgeon [14], in which he took C band measurements at small depression angles from a cliff top in Puerto Rico, and subsequently at Cape Cod, Massachusetts. He observed that the mean Doppler shift for horizontal polarisation is 2 to 4 times as great as that for vertical polarisation in the same wind and wave conditions. He concluded that the vertical polarisation Doppler shift is directly related to the orbital velocity of the gravity waves whereas the horizontal polarisation Doppler shift is directly related to the motion of the surface layer of the sea. For both polarisations, the Doppler shift was directly dependent on the wave height, and varied with the cosine of the angle between the wind and wave direction and the radar look direction. Also he reported that the spectrum bandwidth was relatively independent

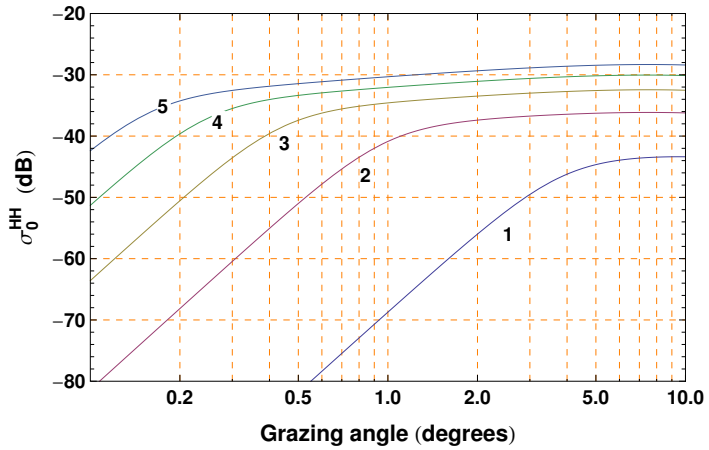

(a) modified GIT model

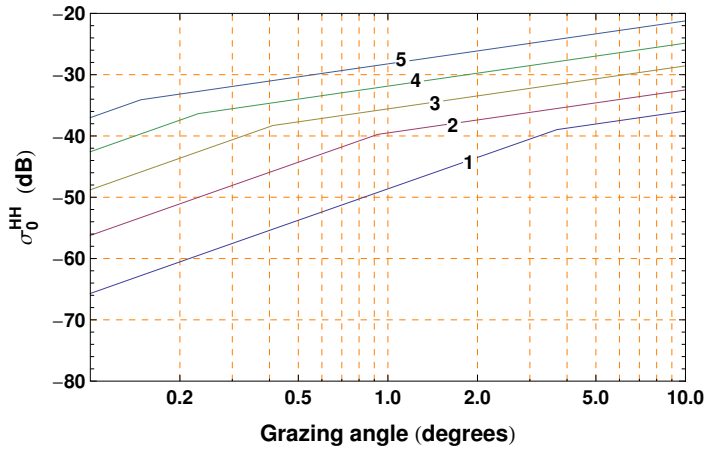

(b) modified Hybrid model

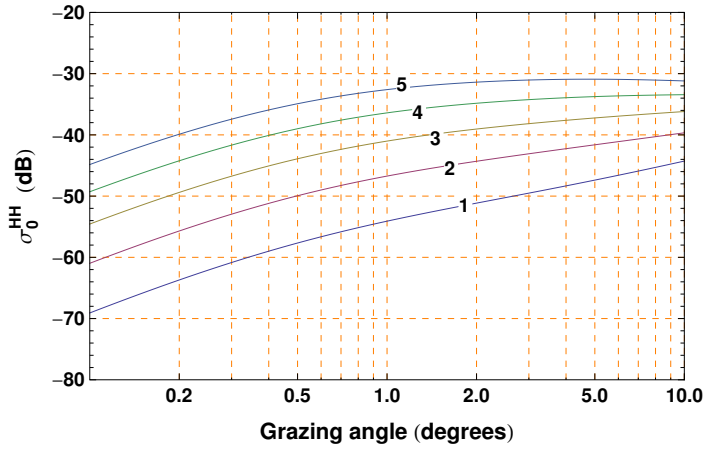

(c) modified NRL model

Figure 1: *Predictions of σ_0^{HH} (m^2/m^2), of the modified models, expressed in dB, as a function of grazing angle, when looking upwind, for sea states 1 to 5, at a frequency of 9300 MHz*

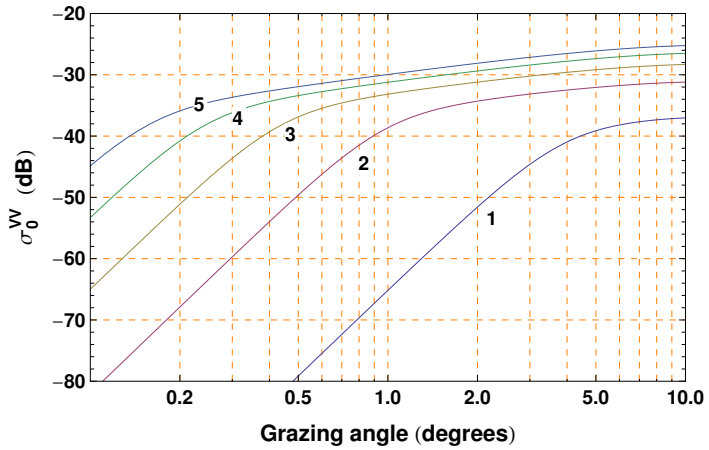

(a) modified GIT model

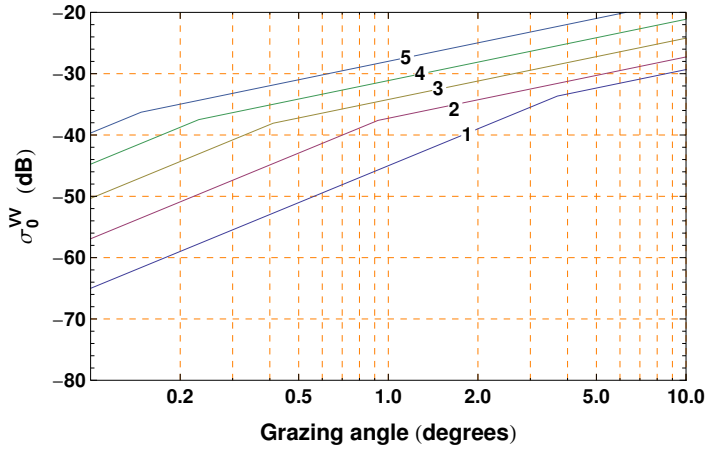

(b) modified Hybrid model

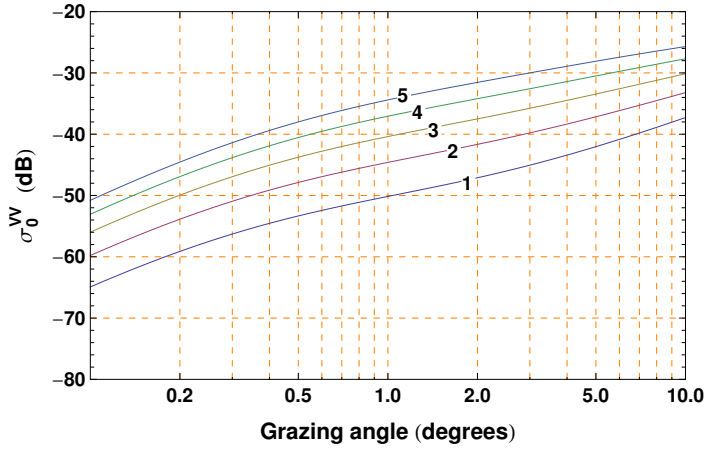

(c) modified NRL model

Figure 2: *Predictions of σ_0^{VV} (m^2/m^2), of the modified models, expressed in dB, as a function of grazing angle, when looking upwind, for sea states 1 to 5, at a frequency of 9300 MHz*

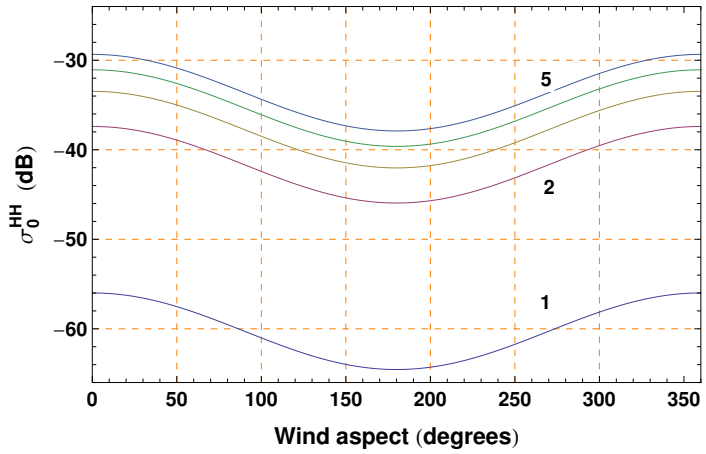

(a) horizontal polarisation

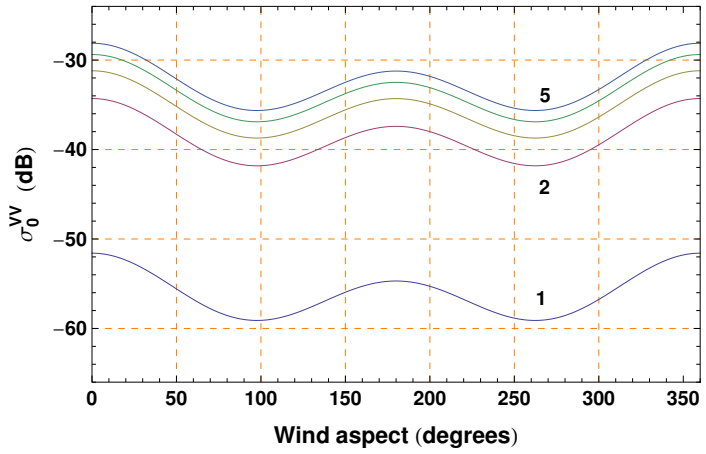

(b) vertical polarisation

Figure 3: *Variation with wind aspect of σ_0^{HH} and σ_0^{VV}, expressed in dB, for the modified GIT model, at a grazing angle of 2°, for sea states 1 to 5, and a frequency of 9300 MHz*

of the viewing angle, but directly dependent on the mean Doppler shift looking into the wind and waves.

With the greater use of Doppler processing in most modern defence radars since the mid 1980s, there has been considerably greater interest in the Doppler properties of sea clutter, to improve the detection characteristics of targets against sea clutter with this class of radars. There are several strands of research that we will follow, notably the work described in the papers of Lee et al., Walker, Rozenberg, and Lamont-Smith.

3.1 Basis Function Decomposition of Sea Clutter Spectra

In 1991, Lee et al, [11] participated in a series of dual polarisation X band measurements of ocean spectra at Loch Linnhe and the Sound of Sleat in the west coast of Scotland, to investigate the physics of microwave backscattering from the ocean surface. A key re-

sult of the investigations was that they were able to differentiate Bragg from non-Bragg scattering, and to resolve the difference between the Doppler structure of vertical and horizontal polarisations. They also reported instances when the amplitude of the horizontal polarisation return exceeds that of vertical polarisation. From their observations of spiking events, they concluded that spiking events can mostly be related to wave breaking events, but can be observed at other times. They suggested that a broader definition of spiking events was required to describe all the observed phenomena than simply stating that it originates from breaking wave events.

Based on the observation that differing phenomena accounted for the spectral components of sea clutter, Lee et al. [10], [12] showed that the clutter spectra could be decomposed into a combination of Gaussian, Lorentzian and Voigtian basis functions. The Gaussian

$$\Psi_G(f) = \frac{1}{W_G\sqrt{\pi}} \exp\left[-\frac{(f-f_G)^2}{{W_G}^2}\right] \tag{36}$$

was used to describe Doppler broadening arising from a spread of scatterer speeds, where f_G is the peak frequency of the spectrum, and W_G is the spectral width. This is typically used to represent Bragg scattering. The Lorentzian was used to describe lifetime or damping-dominated broadening due to finite scatterer lifetime, and is of the form

$$\Psi_L(f) = \frac{\Gamma/2\pi^2}{(f-f_L)^2 + \left(\frac{\Gamma}{2\pi}\right)^2} \tag{37}$$

In this expression, f_L is the peak Doppler frequency of the Lorentzian spectrum, and Γ^{-1} is the characteristic scatterer lifetime. The Voigtian is appropriate if the scattering arises from both lifetime dominated and Gaussian scattering mechanisms, and is a convolution of the two previous profiles,

$$H(a,u) = \frac{a}{\pi}\int_{-\infty}^{\infty} \frac{\exp(-y^2)}{(u-y)^2 + a^2}\, dy \tag{38}$$

in which $a = (f - f_V)/W_G$, f_V is the centre of the Voigt profile, and $a = \Gamma/2\pi W_G$ is the ratio of the Lorentzian full width half maximum to the full width at the $1/e$ level of the Gaussian.

Using the results of the trials at Sound of Sleat referred to above, DRA data from Loch Linnhe that was collected in 1989, and Pidgeon's C band data, they showed that VV data can be represented by a Gaussian profile with a peak at the Bragg resonant frequency, and a Voigtian contributing to the higher frequency wing of the power spectral density. For HH data, the best representation was with a Lorentzian for the principal spectral peak, and a Voigtian contributing to both the upper and lower wings of the spectrum. Some examples of the fit of these functions to the experimental data from [12] are reproduced in Figure 4. Note that in these charts goodness of fit of the functions is judged on a linear scale.

Lee et al. [13] subsequently demonstrated that the basis functions could be applied to laboratory data (i.e. wavetank recordings) as well as ocean data to describe the observed spectra.

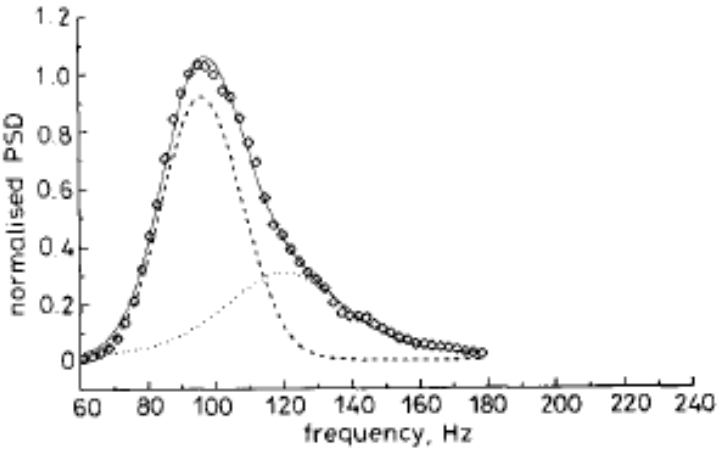

(a) TRW data, vertical polarisation, upwind, wind speed 9 m/s; Gaussian, dashed; Voigtian, dotted; sum of components, solid

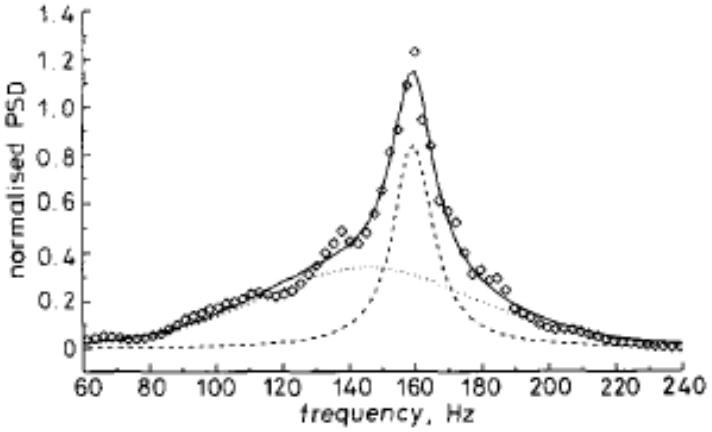

(b) TRW data, horizontal polarisation, upwind, wind speed 9m/s; Lorentzian, dashed; Voigtian, dotted; sum of components, solid

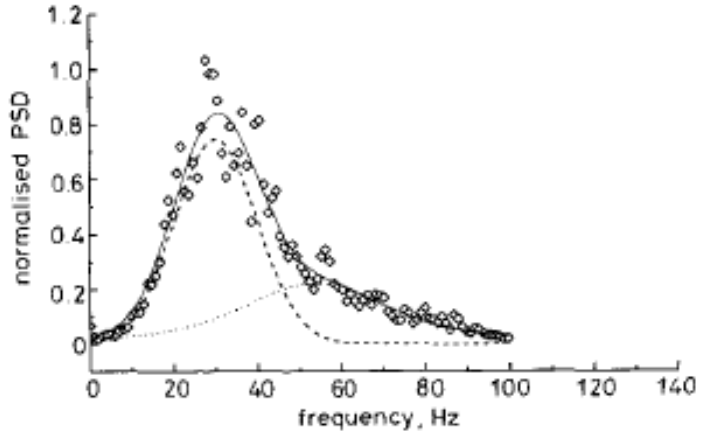

(c) DRA data, vertical polarisation, upwind, wind speed 4 m/s; Gaussian, dashed; Voigtian, dotted; sum of components, solid

Figure 4: *Examples of fitting Gaussian, Lorentzian, and Voigtian basis functions to recorded sea clutter spectra (from Lee et al. [12])*

3.2 Wavetank Investigations of the Doppler Spectra of Waves

At about the same time period as the work of Lee et al., Rozenberg, Quigley and Melville [22], [23] measured the spectra of waves at 14 GHz ($\lambda = 0.021$ m) in a wave tank operated by the Scripps Institution of Oceanography in La Jolla California. The instrumentation enabled simultaneous measurement of the HH and VV polarisation signals, and the amplitude spectrum of the waves. Wind speeds were in the range 2 to 12 m/s, (roughly 4 to 24 knots) and measurements were taken both upwind and downwind at grazing angles of 6°, 8°, and 12°. The main results of interest to us are a series of 4 graphs showing the peak of the Doppler spectrum, and the spectral width versus wind speed for both polarisations as a function of wind speed.

Looking downwind, it is difficult to distinguish the peak Doppler frequencies f of HH and VV polarisation, and there is negligible variation with the incidence angle. The observed Dopplers increase approximately linearly with the wind velocity. Looking upwind the peak Doppler for VV polarisation is very similar to downwind. However, the Doppler for HH polarisation is considerably greater and shows a slight flattening at high wind velocities. Again there is not significant variation with the incidence angle.

The downwind bandwidths, W, of vertical and horizontal polarisation are also difficult to distinguish, and do not vary significantly with grazing angle. Looking upwind, the vertical polarisation bandwidth is roughly linear with frequency up to the limit of the wind velocity measurements, but the horizontal polarisation bandwidth, although linearly proportional for small wind velocities, plateaus to an approximately constant value at about 5 m/s.

The data from these graphs has been digitised and appropriate functions fitted using the *FindFit* function of Mathematica. The data on the peak frequencies of the spectrum, and the functions fitted to the data are shown in Figure 5, and on the bandwidth are shown in Figure 6. No attempt has been made to distinguish the data points from grazing angles of 6°, 8°, and 12° in these figures. The mathematical approximations displayed in the figures are

- Upwind, vertical polarisation $f = 17.36 + 10.59U^{0.29} + 0.0153U^{3.05}$
- Upwind, horizontal polarisation $f = -39.43 + 57.48\sqrt{U} - 5.69U$
- Downwind, both polarisations $f = 22.83 + 2.84U$
- Upwind vertical polarisation $W = 5.28U$
- Upwind, horizontal polarisation $W = \mathrm{Min}(6.15\,U, 36.7)$
- Downwind, both polarisations, $W = 3.92U$

where U is the wind speed in metres/second, and Min is the minimum value of the enclosed parameters. Note that these results need to be appropriately scaled to provide estimates of the position of the spectral peak and bandwidths at radar frequencies other than that used in these measurements.

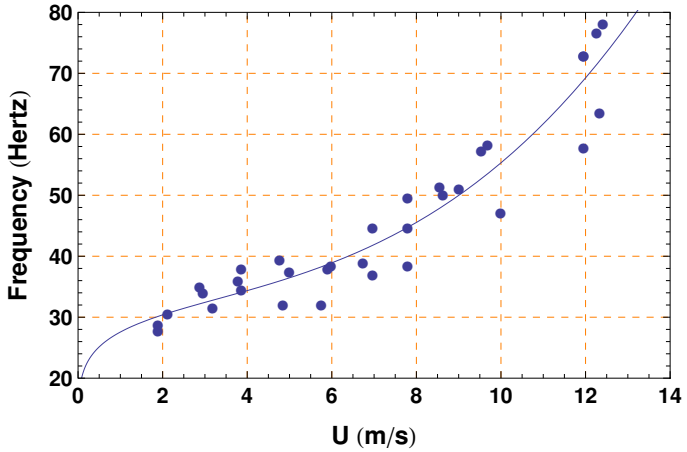

(a) vertical polarisation, upwind

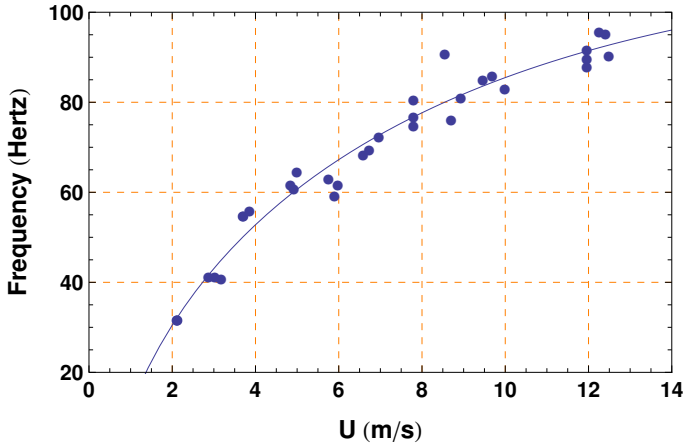

(b) horizontal polarisation, upwind

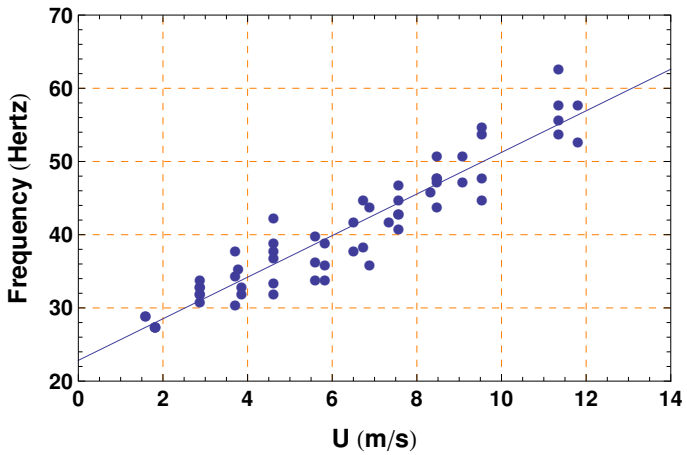

(c) downwind, both polarisations

Figure 5: *Peak frequency of Doppler spectrum at 14 GHz as a function of windspeed, data points from [22], solid line - best fit of mathematical model*

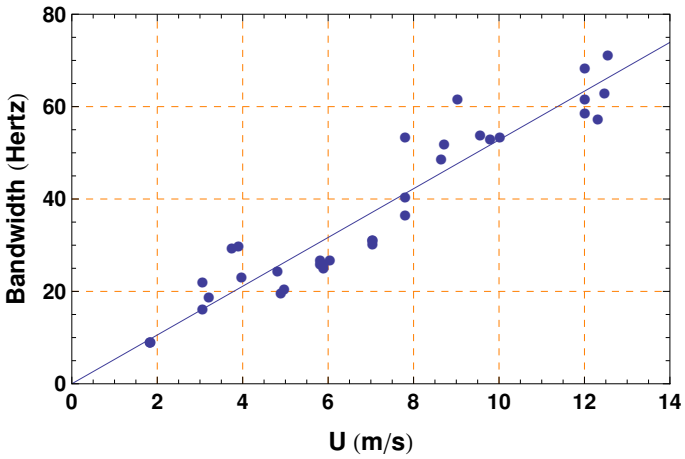

(a) vertical polarisation, upwind

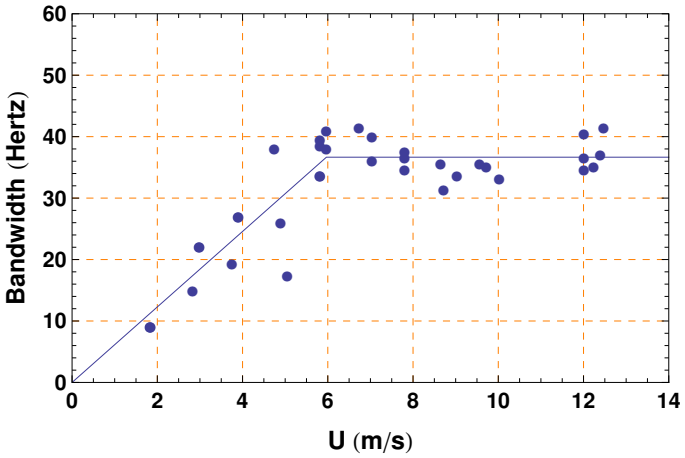

(b) horizontal polarisation, upwind

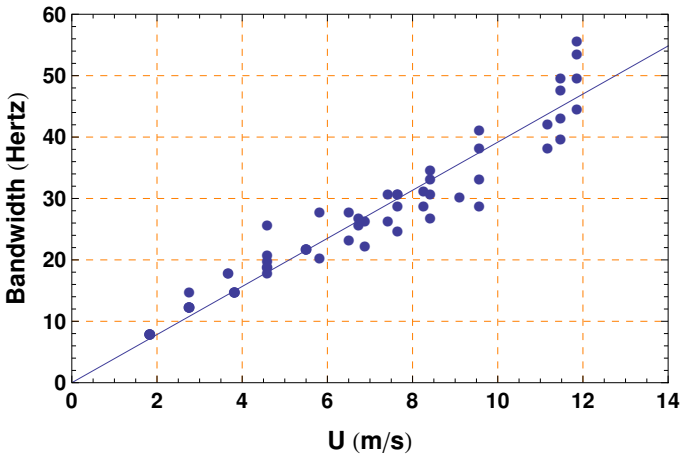

(c) downwind, both polarisations

Figure 6: *Bandwidth of Doppler spectrum at 14 GHz as a function of windspeed, data points from [22], solid line - best fit of mathematical model*

3.3 Doppler Measurements of Ocean Waves

The papers of Pidgeon and of Valenzuela on the measurement of the spectra of ocean sea clutter, while instructive on the characteristics of the spectra, do not contain sufficient detail to develop a model. However in 2000, Walker [27] published a three component model to describe wave tank measurements similar to that of Lee et al. above, and then applied this model to ocean data recorded in 1996 from a clifftop known as Portland Bill on the south coast of England [26]. From the wavetank work, Walker identified three different mechanisms that contributed to the scattered signal

1. Bragg scattering, arising from scattering by the capillary waves riding on the longer gravitational waves, both polarisations peaking at the same frequency, and being significantly greater in magnitude for VV polarisation than for HH polarisation
2. scattering from rough whitecaps of broken waves, of roughly equal magnitude for both polarisations, and speed significantly higher than the Bragg scattering
3. specular scattering from the crest of waves, termed spikes, and prominent in HH polarisation, but not significant in VV, with a Doppler close to that of the whitecaps

Each component is assigned a Gaussian distribution. For vertical polarisation, the model is of the form

$$\Psi_V(f) = P_B^V \exp\left(\frac{-(f-f_B)^2}{{W_B}^2}\right) + P_W \exp\left(\frac{-(f-f_W)^2}{{W_W}^2}\right) \tag{39}$$

whereas for horizontal polarisation

$$\Psi_H(f) = P_B^H \exp\left(\frac{-(f-f_B)^2}{{W_B}^2}\right) + P_W \exp\left(\frac{-(f-f_W)^2}{{W_W}^2}\right) + P_S \exp\left(\frac{-(f-f_W)^2}{{W_S}^2}\right) \tag{40}$$

In these expressions, subscripts B, W, and S refer respectively to the Bragg, whitecap and spike components. Thus f is the radar Doppler frequency, f_B and f_W are the Doppler frequencies corresponding to the phase velocity of the Bragg resonant and dominant gravity waves giving rise to the whitecaps, and W_B and W_W are the widths of the corresponding spectra. P_B^V and P_B^H are the amplitudes of the vertical and horizontal Bragg components, whereas P_W and P_S are the whitecap and spike components. Note that the whitecap component is the same in both polarisations, and that the spike component has the same Doppler peak as the whitecap component, though a different spectral width. In comparison with Lee et al. above, the use of Gaussian functions for each component provides very good correlation with measurements to low signal levels when compared on a logarithmic (dB) scale.

Two sets of data acquired at Portland Bill on separate days are presented in the paper. The radar operated at a centre frequency of 9.75 GHz, at 64 m above mean sea level, with a grazing angle of 3.6°. The data are averaged over a time period of 30 seconds. The first set is with the radar looking directly into the wind, with a windspeed of 10 m/s, gusting to 15 m/s. The second set is with the radar looking downwind, with a windspeed at 7 m/s, gusting to 10 m/s. The difficulty with the measurements is that detailed information on the surface could not be obtained, which meant that many surface parameters were unknown

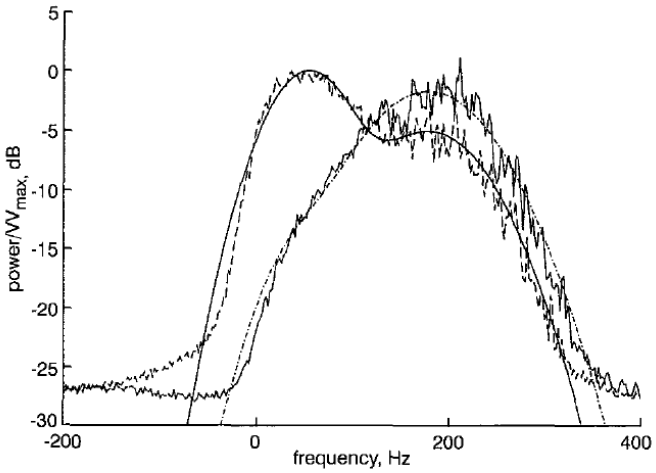

Figure 7: *Three component model applied to upwind data, solid-VV model, dashed-HH model (from Walker [26])*

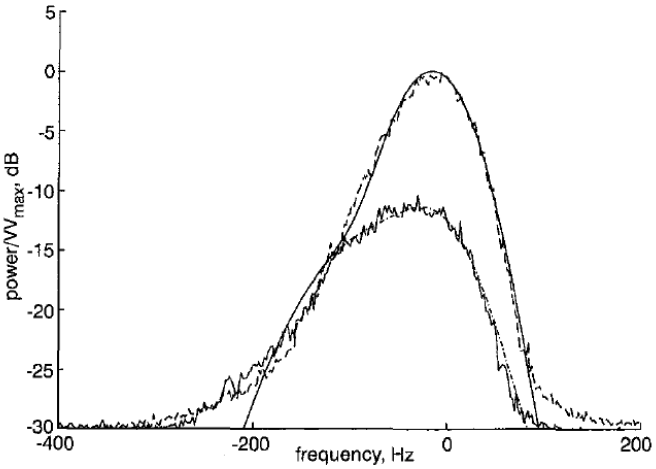

Figure 8: *Three component model applied to downwind data, solid-VV model, dashed-HH model (from Walker [26])*

and had to be inferred from the data. In the upwind VV data, the Bragg component is clearly visible, and the whitecap component at a higher frequency is only slightly lower in amplitude. In the HH data, the Bragg component is evident as a slight bump in the curve. The HH peak exceeds the VV curve at this point indicating a contribution from both the whitecap and spike components in these measurements. The downwind spectra look quite different, without any clear peak separation, and nowhere does HH significantly exceed VV. The Bragg peaks provide the greater components of the spectrum with the whitecap component much smaller. The spike term does not contribute to the downwind measurements. Upwind P_W is typically 4 to 10 dB below P_B^V, and downwind about 14 dB below B_V [26], [27]. The model parameters Walker extracted from the data using a Powell minimisation algorithm are listed in Table 4. Figures 7 and 8 show the level of agreement with the data of the three component model for the upwind and downwind data respectively for these parameters.

Table 4: *Model Parameters for Upwind and Downwind Data from Portland Bill [26]*

	P_B^H/P_B^V	P_W/P_B^H	P_S/P_B^H	f_B(Hz)	f_G(Hz)	W_B(Hz)	W_W(Hz)	W_S(Hz)
Upwind	-15.1 dB	11.5 dB	12.8 dB	54	178	47.5	66.0	74.5
Downwind	-14.0 dB	0.2 dB	-	-15.3	-63.9	40.4	74.1	-

4 Constructing a Doppler Model of Sea Clutter

There is no published model which satisfies our requirement for estimating the performance of maritime surveillance modes of coherent pulse Doppler radars, but there are many different pieces of information that when combined will allow us to proceed with this task in a qualified way. We make the following remarks

1. Walker's model using Gaussian functions appears to be quite appropriate for describing the spectral characteristics of the ocean conditions of interest; it provides good results over a significant dynamic range, and is simpler to implement than the model of Lee et al. A key feature of this model is that the whitecap component is the same magnitude for both polarisations.

2. Rozenburg did not distinguish the origins of the different spectral components in his wave tank measurements, but we might reasonably conclude from applying Walker's conclusions to his charts that

   (a) in the upwind vertical polarisation measurements, the peak in the wave tank spectra will be due to the Bragg component, and the width essentially the Bragg width

   (b) in the upwind horizontal polarisation measurements, the peak in the wave tank spectra will be essentially due to the whitecap component, and the width likewise

   (c) in the downwind vertical polarisation measurements, the peak in the wave tank spectra will be due to the Bragg component, and the width essentially the Bragg width

   (d) in the downwind horizontal polarisation measurements, the peak in the wave-tank spectra will be due to the Bragg component, but the width will be broadened due to the presence of the almost equal amplitude whitecap component

3. We now need to establish the positions and beamwidths of the Bragg and whitecap terms as a function of aspect angle.

   (a) Scaling Rozenburg's measurements of the Bragg spectrum peak for the radar wavelength λ (m) of interest, from the upwind measurements we have

   $$f_B^u = \left(17.36 + 10.59\,U^{0.29} + 0.0153\,U^{3.05}\right)\,0.021/\lambda \tag{41}$$

   whereas from the downwind measurements

   $$f_B^d = (22.83 + 2.84\,U)\,0.021/\lambda \tag{42}$$

where superscripts u, and d indicate upwind and downwind directions. At broadside the Doppler of the Bragg component should be 0, so an appropriate function for the angular dependence of the Doppler might be

$$f_B = \begin{cases} f_B^u \cos\phi, & 0 \le \phi \le \pi/2, \\ f_B^d \cos\phi, & \pi/2 \le \phi \le \pi \end{cases} \tag{43}$$

Note that this correctly accounts for the sign of the Doppler for downwind cases.

(b) For the whitecap term from the upwind measurements the peak Doppler is

$$f_W^u = \left(-39.43 + 57.48\sqrt{U} - 5.69U\right) 0.021/\lambda \tag{44}$$

and from the downwind measurements

$$f_W^d = (22.83 + 2.84\,U)\, 0.021/\lambda \tag{45}$$

Again zero Doppler is expected at broadside, so an appropriate angular dependence is

$$f_W = \begin{cases} f_W^u \cos\phi, & 0 \le \phi \le \pi/2, \\ f_W^d \cos\phi, & \pi/2 \le \phi \le \pi \end{cases} \tag{46}$$

(c) The bandwidth of the Bragg component follows from the upwind vertical polarisation measurements

$$W_B^u = 5.28U \tag{47}$$

and for downwind

$$W_B^d = 3.92U \tag{48}$$

Combining these results with a sinusoidal transition provides

$$\begin{aligned} W_B &= \frac{W_B^u + W_B^d}{2} + \frac{W_B^u - W_B^d}{2}\cos\phi \\ &= (4.6 + 0.68\,U\cos\phi)\, 0.021/\lambda \end{aligned} \tag{49}$$

(d) The bandwidth of the whitecap component follows from the horizontal polarisation measurements. Upwind we have

$$W_W^u = \begin{cases} 6.15\,U & U < 5.97 \\ 36.7, & U > 5.97 \end{cases} \tag{50}$$

and downwind,

$$W_W^d = 3.92U \tag{51}$$

Combining these results in a smooth transition with angle

$$W_W = \begin{cases} (5.035 + 1.115\cos\phi)\, U\, 0.021/\lambda & U < 5.97 \\ (18.35 + 1.96\,U + (18.35 - 1.96\,U)\cos\phi)\, 0.021/\lambda & U > 5.97 \end{cases} \tag{52}$$

(e) Walker records that the spectral width of the spike component is slightly greater than the whitecap component by a factor of 1.13 at a windspeed of 10 m/s. Hence we shall assume

$$W_S = 1.13\, W_W \tag{53}$$

(f) We note at this stage that it may be necessary to scale the above frequency and bandwidth estimates as they are typically much greater in recorded ocean data than in data obtained from wavetank measurements.

4. We have been discussing spectral power densities, but clutter models such as the GIT model supply average cross sections. Integrating Walker's spectral model over frequency we find that

$$\sigma_{VV} = \sqrt{\pi}\,(W_B\, P_B^V + W_W\, P_W) \tag{54}$$

and

$$\sigma_{HH} = \sqrt{\pi}\,(W_W\, P_B^H + W_W\, P_W + W_S\, P_S) \tag{55}$$

Since there are four unknowns, it is not possible to directly determine the spectrum parameters from σ_{VV} and σ_{HH} alone, so further assumptions are required about the relative magnitudes of the parameters to reduce the unknowns to two. There are two methods which have been investigated.

4.1 Method 1

Beginning with data for the horizontal polarisation cross section of sea clutter, the ratios of the Bragg, whitecap and spike terms must first be estimated, and then they can be evaluated from σ_{HH}. Assuming equality of the whitecap component in both polarisations, the Bragg component of the vertical polarisation cross section can be calculated by subtracting the whitecap power from σ_{VV}.

Treating the spike component P_S in Equation 55 first, looking upwind at a wind speed of 10 m/s, Walker's data indicates that the spike exceeds the horizontally polarised Bragg term by 12.8 dB, a factor of 19.1. But at 5 m/s, spikes are rare so we might model the ratio to diminish to 0 at 4 m/s. Also we note that sea spikes are highly directional and do not exist in the downwind sector. Thus, they might be modelled as

$$\begin{aligned} \left.\frac{P_S}{P_B^H}\right|_\phi &= \text{Max}\left[0,\, 19.1\left(\frac{U-4}{6}\right)\right]\cos\phi, && 0 \le \phi \le \pi/2, \\ &= 0, && \pi/2 \le \phi \le \pi \end{aligned} \tag{56}$$

where U is the wind strength in metres per second. The Max function is used to set the spike component to 0 for wind velocities less than 4 m/s, and the cosine function reduces the ratio to 0 at $\phi = \pi/2$. To reduce the ratio more quickly with aspect we could consider using the second or a higher power of the cosine function.

The horizontally polarised Bragg component is generally small compared with the whitecap component when looking in the upwind direction, but downwind these components are roughly equal. Walker's upwind data indicates that at 10 m/s, the ratio of P_W

to P_B^H is 11.5 dB, or a factor of 14.1. Looking downwind, the ratio is 1.05 (0.2 dB) at 7 m/s in Walkers data. We might reasonably assume, in the absence of any other data, that these ratios will diminish in proportion to the wind velocity since wavebreaking does not occur in low sea states. Finally we need to transition the ratio from its upwind value to its downwind value by a smooth function, and thus we might use

$$\left.\frac{P_W}{P_B^H}\right|_\phi = 14.1\,\frac{U}{10}\left(\frac{1+\cos\phi}{2}\right) + 1.05\,\frac{U}{7}\left(\frac{1-\cos\phi}{2}\right) \tag{57}$$

in our model.

Now given σ_{HH} from the clutter model, we can determine P_B^H from Equation 55, thus

$$P_B^H = \frac{\sigma_{HH}}{\sqrt{\pi}\left(W_b + W_W\frac{P_W}{P_B^H} + W_S\frac{P_S}{P_B^H}\right)} \tag{58}$$

The values of P_W and P_S then immediately follow from Equations 57 and 56. Then rearranging Equation 54, P_B^V can be determined from

$$P_B^V = \frac{\sigma_{VV} - \sqrt{\pi}\,W_W P_W}{\sqrt{\pi}\,W_B} \tag{59}$$

A major difficulty with this model is that near broadside the power in the whitecap component $\sqrt{\pi}\,W_W P_W$ determined from σ_{HH} exceeds σ_{VV} at higher sea states, and so the predicted value of P_B^V is negative. The solution that gives acceptable results is to increase the power in the spike component near broadside, thus reducing the whitecap term. This has been achieved by setting the spike component to transition to 0 at $\phi = \pi$ instead of $\pi/2$, thus

$$\left.\frac{P_S}{P_B^H}\right|_\phi = \mathrm{Max}\left[0,\, 19.1\,\left(\frac{U-4}{6}\right)\right]\left(\frac{1+\cos\phi}{2}\right) \tag{60}$$

in the model, though transitioning to 0 at $\phi = 3\,\pi/4$ is also satisfactory. It might be argued that spikes do not exist in the downwind sector, and so the model is not correct, but the problem may also be attributed to imprecision in determining the differences between vertical and horizontal polarisation in the clutter model(s). Regardless, the total power of the clutter model used to determine the spectral components is preserved.

4.2 Method 2

In this method, we begin the analysis with σ_{VV} to determine P_B^V and P_W from the ratio of these terms, and then determine P_B^H from its ratio to P_W. The spike term is then calculated from the remainder of σ_{HH} after the whitecap and horizontal Bragg components are subtracted from it. Walker [26] records for the data sets he analysed that upwind at a wind speed of 10 m/s, the ratio of P_W to P_B^V is 0.437 (-3.6 dB), and downwind at 7 m/s, the ratio is 0.0417 (-13.8 dB). If we assume that these ratios are proportional to the wind speed, i.e. an increased wind speed increases the whitecap component proportionally, and we use a smooth cosine function to transition from upwind to downwind, then

$$\left.\frac{P_W}{P_B^V}\right|_\phi = 0.437\,\frac{U}{10}\left(\frac{1+\cos\phi}{2}\right) + 0.0417\,\frac{U}{7}\left(\frac{1-\cos\phi}{2}\right) \tag{61}$$

Rearranging Equation 54

$$P_B^V = \frac{\sigma_{VV}}{\sqrt{\pi}\left(W_B + W_W \frac{P_W}{P_B^V}\right)} \tag{62}$$

and then P_W can be determined from Equation 61. Likewise P_B^H can be determined from Equation 57; it is interesting to note that no information about σ_{HH} is used in this method to determine the horizontal Bragg component. The spike term then follows from

$$P_S = \frac{\sigma_{HH} - \sqrt{\pi} W_B P_B^H - \sqrt{\pi} W_W P_W}{\sqrt{\pi} W_S} \tag{63}$$

4.3 Scaling the Wavetank Data Model

Open ocean spectral data appears greater in frequency and wider in bandwidth than data obtained from wavetanks. To obtain spectra that are comparable with Walker's upwind and downwind examples, the models for the frequencies and bandwidths from the wavetank data need to be scaled up. In doing this we note that the ocean around Portland Bill has strong currents which may influence the Doppler frequencies, particularly the frequency of the Bragg components of vertical and horizontal polarisation. The factors that were selected by visual comparison of the spectra, and are used to modify Equations 41 through 52, are

1. Bragg peak frequency factor - 1.3
2. Whitecap peak frequency factor - 2.7 looking upwind, 2.3 looking downwind
3. Bragg bandwidth factor - 1.3
4. Whitecap bandwidth factor - 2.7

The frequency of the spike component is the same as the whitecap component, and its bandwidth is set at 1.13 times the whitecap bandwidth.

5 Predictions of Sea Clutter Spectral Components

Figures 9 to 12 show each of the clutter spectral components obtained from the three modified clutter models discussed earlier. Both parameter extraction methods are compared over sea states 1 to 5, as a function of wind aspect. In all these figures, the frequency is 9300 MHz, and the grazing angle is 2°. Note that for the spike component (Figure 12) for method 1 only sea states 2 to 5 are displayed as the spike component is set to 0 for wind strengths less than 4 m/s.

The horizontal polarisation Bragg spectral density, (Figure 9), shows a significant difference between the two methods. In method 2, the horizontal polarisation has the bimodal characteristics of σ_{VV} although σ_{HH} is unimodal in the clutter models. The

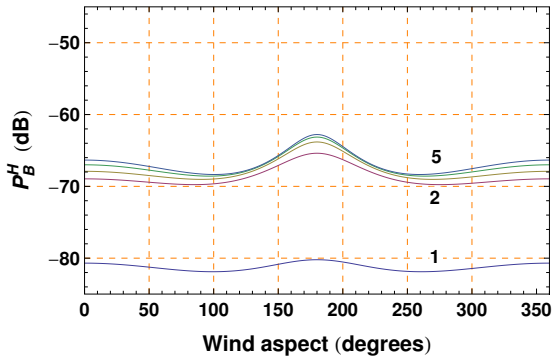

(a) modified GIT, method 1

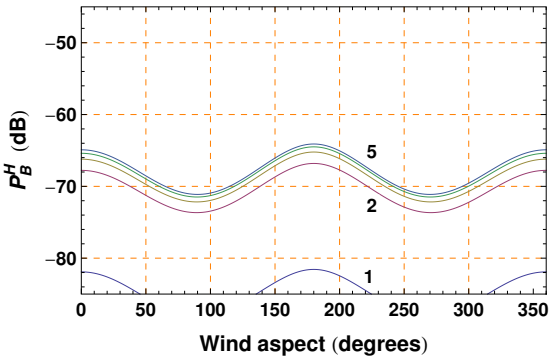

(b) modified GIT, method 2

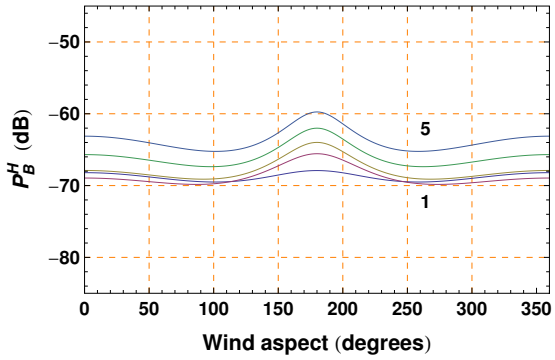

(c) modified Hybrid, method 1

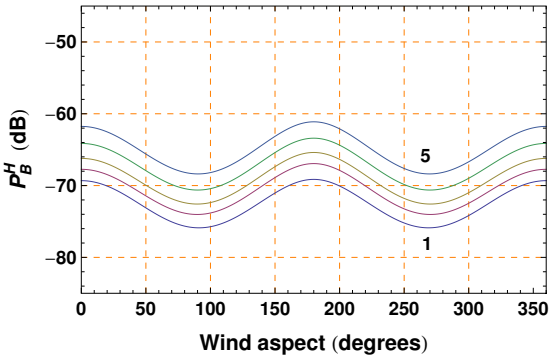

(d) modified Hybrid, method 2

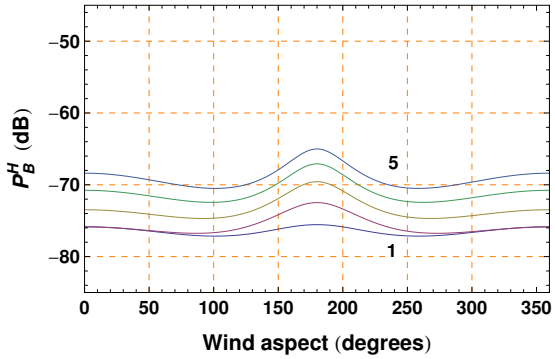

(e) modified NRL, method 1

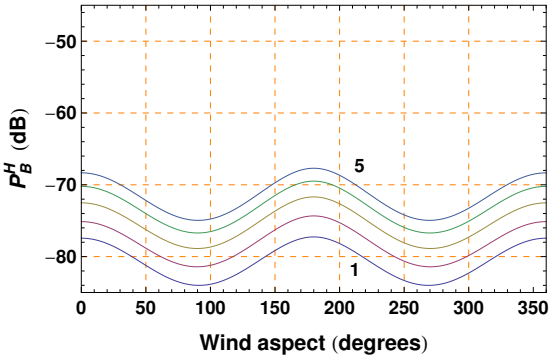

(f) modified NRL, method 2

Figure 9: *Bragg component of horizontal polarisation clutter spectral power density* $(m^2/m^2/Hz)$*, expressed in dB, as a function of wind aspect* ϕ *at 9300 MHz for sea states 1 to 5, at a grazing angle of* 2°

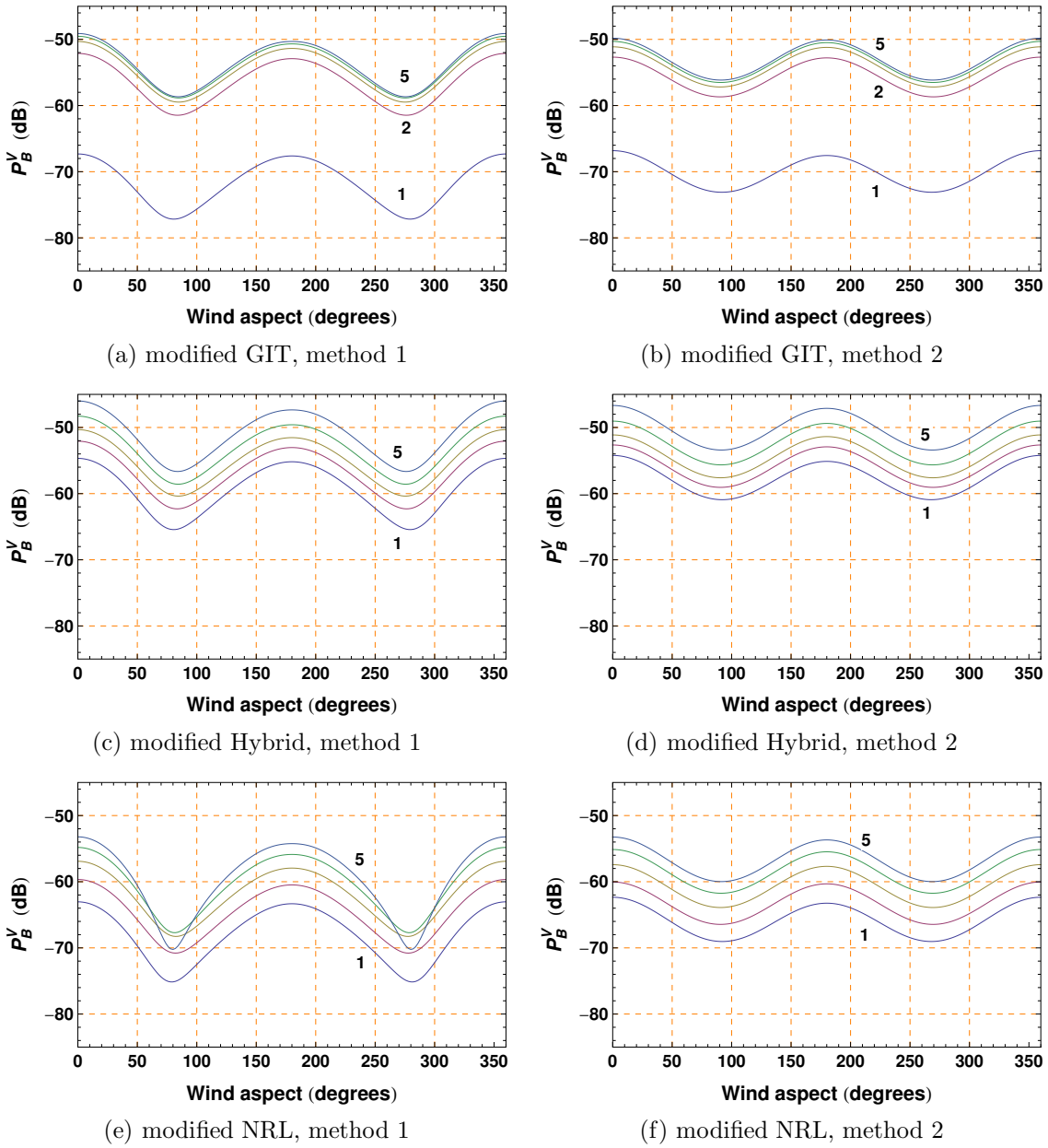

(a) modified GIT, method 1

(b) modified GIT, method 2

(c) modified Hybrid, method 1

(d) modified Hybrid, method 2

(e) modified NRL, method 1

(f) modified NRL, method 2

Figure 10: *Bragg component of vertical polarisation clutter spectral power density ($m^2/m^2/Hz$), expressed in dB, as a function of wind aspect ϕ at 9300 MHz for sea states 1 to 5, at a grazing angle of* 2°

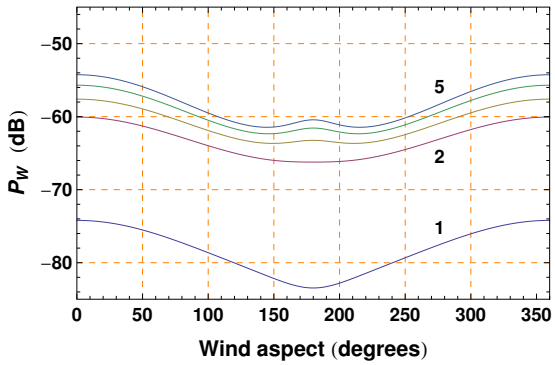

(a) modified GIT, method 1

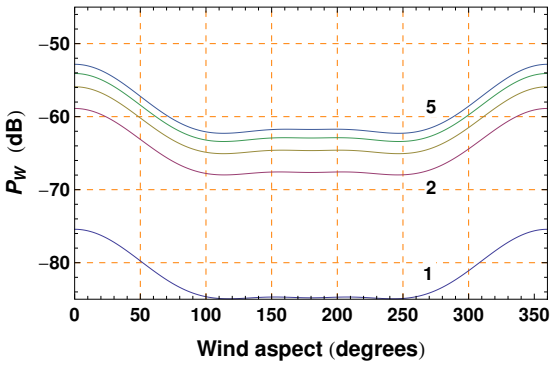

(b) modified GIT, method 2

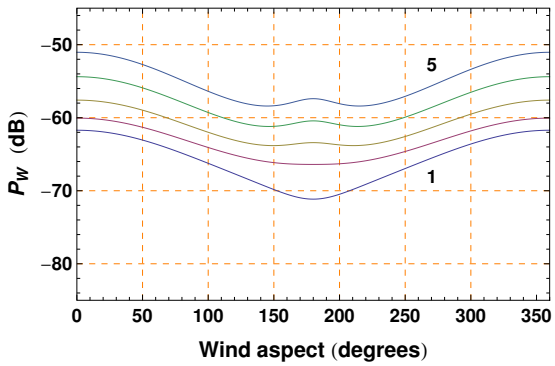

(c) modified Hybrid, method 1

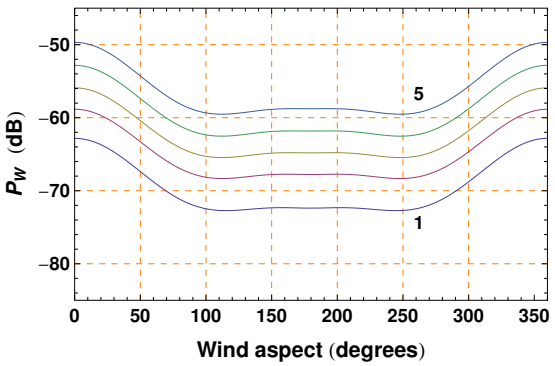

(d) modified Hybrid, method 2

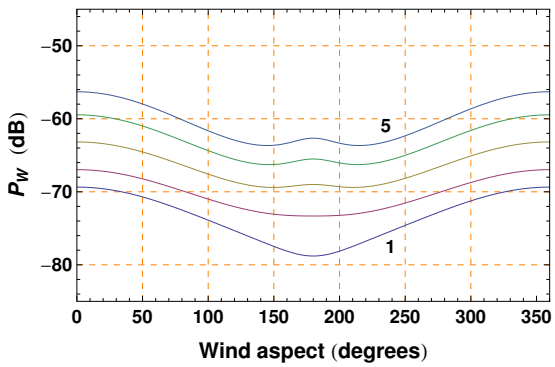

(e) modified NRL, method 1

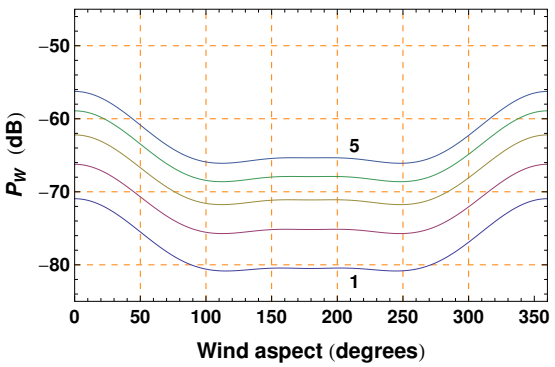

(f) modified NRL, method 2

Figure 11: *Whitecap component of clutter spectral power density ($m^2/m^2/Hz$), expressed in dB, as a function of wind aspect ϕ at 9300 MHz for sea states 1 to 5, at a grazing angle of* 2°

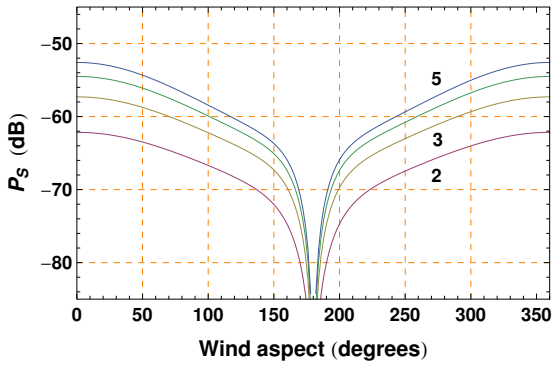

(a) modified GIT, method 1

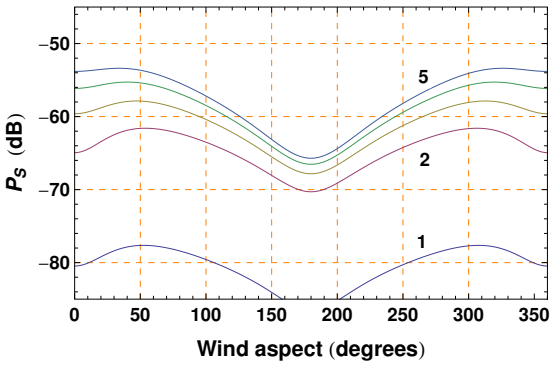

(b) modified GIT, method 2

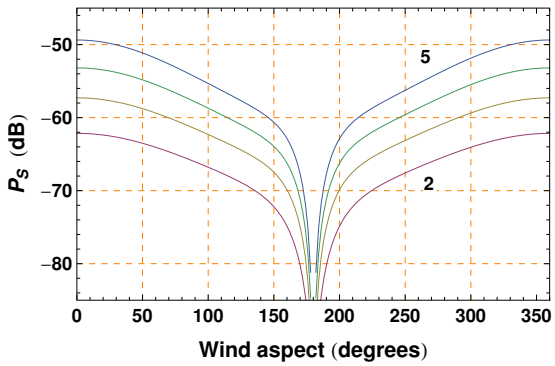

(c) modified Hybrid, method 1

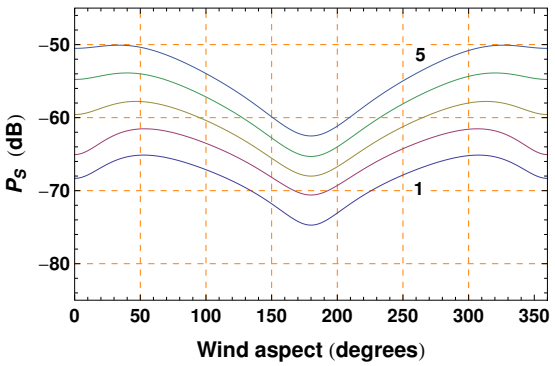

(d) modified Hybrid, method 2

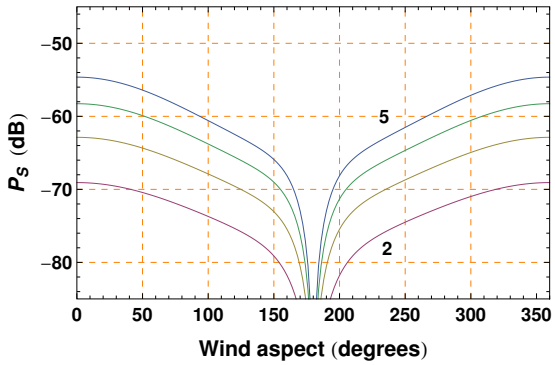

(e) modified NRL, method 1

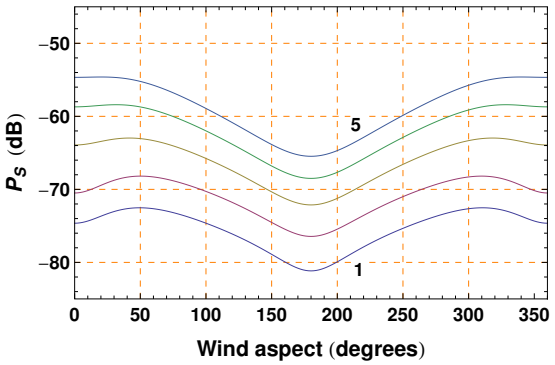

(f) modified NRL, method 2

Figure 12: *Spike component of horizontal polarisation spectral power density ($m^2/m^2/Hz$), expressed in dB, as a function of wind aspect ϕ at 9300 MHz for sea states 1 to 5, at a grazing angle of* 2°

explanation for this is that in this method, P_B^H is in the vicinity of 15 dB less than P_B^V for all aspects and so is also bimodal. The method 1 predictions are quite different, with only about a 2 dB decrease with increasing aspect angle until the downwind sector where it rises sharply by about 6 to 8 dB. Even for sea state 1, for which there is no spike component, there is still a slight peak in the downwind direction. Even though the horizontal Bragg component has been entirely deduced from σ_{HH}, which is unimodal, the peak in the downwind direction implies a bimodal component in the spectrum. With regard to the spacing of the different sea states, with the modified GIT model, the lines for sea states 2 to 5 are tightly bunched together, with sea state 1 quite distinct about 12 dB less in amplitude, for both methods. Note also that with the modified Hybrid and modified NRL models using method 1, the lines for sea states 1 and 2 almost coincide except for downwind aspects. With method 2, the spacing of the Bragg lines obtained from the modified hybrid and modified NRL models corresponds more closely to the spacing in the respective clutter models.

The vertical polarisation Bragg component, (Figure 10), being mostly larger than the whitecap component, closely follows the characteristics of σ_{VV}. For all three clutter models, the variation in amplitude with aspect for method 1 is greater than that obtained with method 2, but otherwise quite similar. Bunching of the curves is again seen for the modified GIT model, but both the modified Hybrid and modified NRL models produce quite regularly spaced sea state lines. However the modified NRL model with method 1 shows unusual behaviour with a large reduction in amplitude for higher sea states near the crosswind look direction, resulting in the sea state 5 curve crossing both sea state 4 and 3 curves, and almost touching the sea state 2 curve in this region. There appears to be no a priori reason why the amplitude of the Bragg line should be monotonic with sea state in this region; a possible explanation could be that the larger wave action of sea state 5 with associated whitecaps might have a substantial effect on propagation of the Bragg component in the crosswind direction, thus resulting in the dip seen with method 1. In the absence of definitive data on the spectral characteristics of the clutter, it is difficult to decide whether the predictions on method 1 with the modified NRL data should be rejected.

The Walker model of sea clutter assumes that the whitecap component of sea clutter is identical for both polarisations. Beginning first with the development of the whitecap component from σ_{HH} of method 1, we see that the amplitude is quite closely unimodal except of a slight peak in the higher sea states in the downwind direction. The predictions for method 2 are quite different. Initially the amplitude decreases at the rate of a bimodal waveform but in the downwind sector is almost constant from about 100° to 250°.

In method 1, the spike component (Figure 12) is forced to 0 in the downwind direction, but in method 2 is allowed to account for the remainder of σ_{HH} after determining the Bragg and whitecap components, and so is significantly different; in the latter the downwind component is about 12 dB below the upwind level for all clutter models. It is questionable whether a spike component exists in the downwind sector, but it is necessary to include this in the spectral model so that the whitecap component is the same for both vertical and horizontal polarisation for both methods. It may be that this is merely a problem inherent in the averaging of the clutter data in each polarisation in generating the clutter models we used in our analysis.

When we look at the total spectra, the results from the different clutter models are quite similar in form, and we have elected to show only the results obtained with the modified NRL clutter model. Figure 13 shows the combined spectra for horizontal polarisation for both methods for sea states 1, 3 and 5 at a grazing angle of 2° for wind aspects in 45° increments between upwind and downwind. Reasonable correspondence is obtained with Walker's measurements. The Bragg term is relatively insignificant and mainly manifests itself as a slight bump in the lower half of each spectrum curve. In the vertical polarisation curves (Figure 14) the Bragg term is dominant, especially at low sea states. Close correspondence with Walker's measurements is achieved with a sea state of 4.22, for which the wind velocity is 10 m/s, according to the relationship between wind velocity and sea state used in the clutter model.

The differences between the spectra obtained with the two methods are relatively minor but it is not known whether they are significant in detection calculations.

6 Conclusions

This investigation has demonstrated that it is possible to deduce a credible spectrum for sea clutter from standard total cross section sea clutter models, with the support of a set of assumptions about the relative relationship of the components that comprise the sea clutter spectrum. However, it has generated as many questions as it has answered; all the results appear acceptable, and the different generating clutter models will need to be used advisedly for the purpose to which the spectrum data is to be put. In carrying out this investigation, the modified NRL model has some features which might make it more suitable for this use; in particular, the vertical and horizontal polarisation terms are separately optimised to conform with Nathanson's data, not relying upon a fixed dB difference independent of sea state, as used in the other two models, which may be significant in determining the spectral components. Also the much improved accuracy at low sea states is significant for the requirement for which the model was developed.

An experimental measurement program which investigates the validity of the assumptions in deriving these results is warranted as there is a need for accurate low grazing angle Doppler sea clutter models across a number of Defence programs. In particular there is need for the measurement of the separate terms comprising the spectrum, to determine their ratio at various wind strengths and a wide range of aspect angles, as the predictions of this research depend on these ratios. It is also desirable to confirm Walker's model, that the whitecap component is identical for both polarisations, for all aspects, as it does not seem justified from an electromagnetic scattering perspective. Data is also required on the behaviour of the spike component, particularly its dependence on the wind aspect angle and whether it is present in the downwind sector.

It is hoped that this model will prove useful for more applications than the specific project which it was developed, as it is an appropriate tool to assist in the assessment of performance of a number of radar systems of current interest to Defence. Given the highly speculative nature of the development of this model, it is anticipated that the assumptions and the methods for deducing the spectral components will evolve as new data comes available.

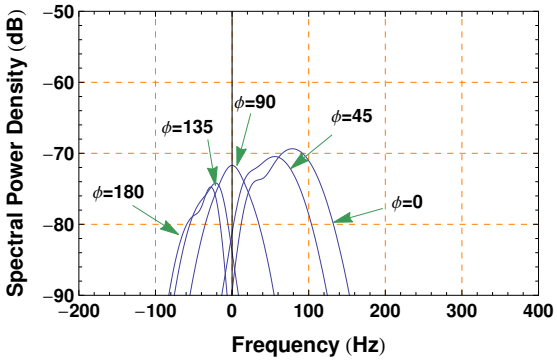

(a) sea state 1, method 1

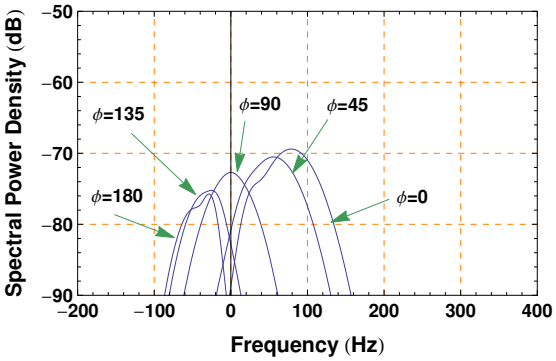

(b) sea state 1, method 2

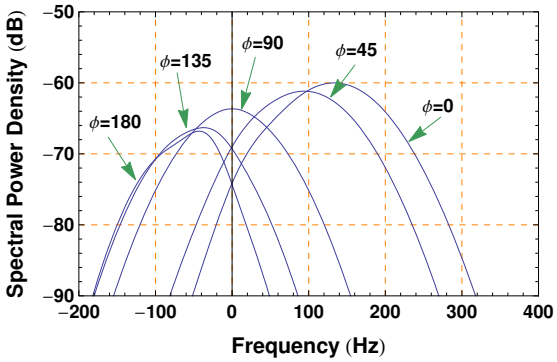

(c) sea state 3, method 1

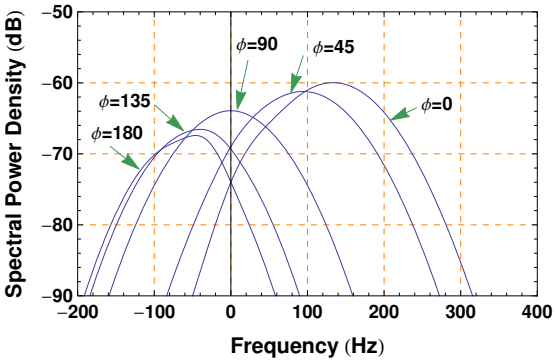

(d) sea state 3, method 2

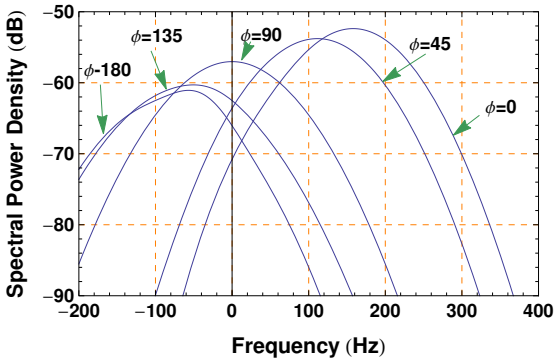

(e) sea state 5, method 1

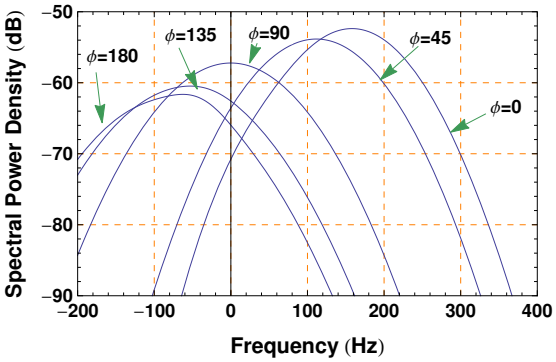

(f) sea state 5, method 2

Figure 13: *Predicted power spectral density ($m^2/m^2/Hz$), expressed in dB, of horizontal polarisation sea clutter at 9300 MHz, using the modified NRL clutter model, at a grazing angle of* 2°*, for wind aspect* ϕ *between* 0° *and* 180°

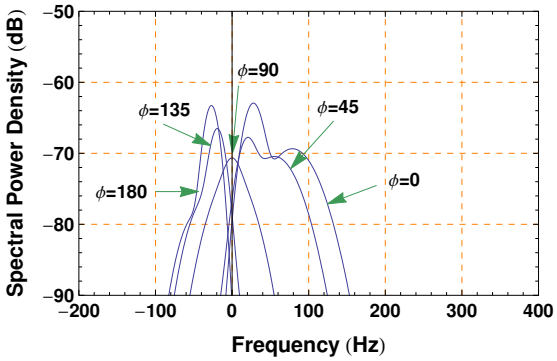

(a) sea state 1, method 1

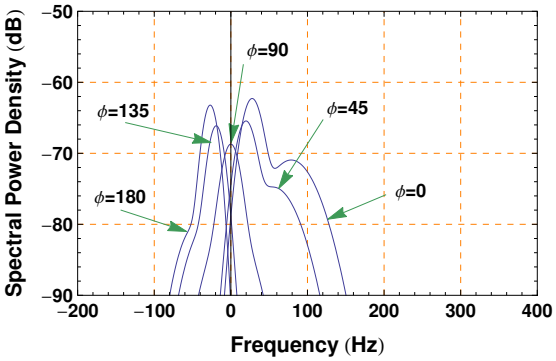

(b) sea state 1, method 2

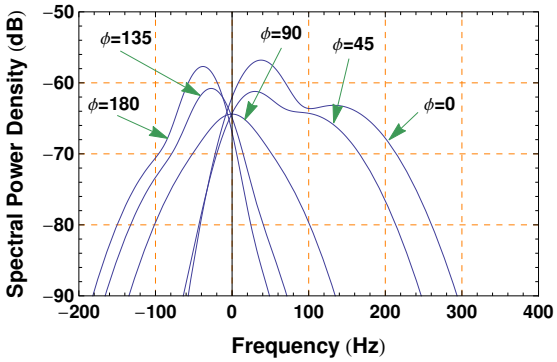

(c) sea state 3, method 1

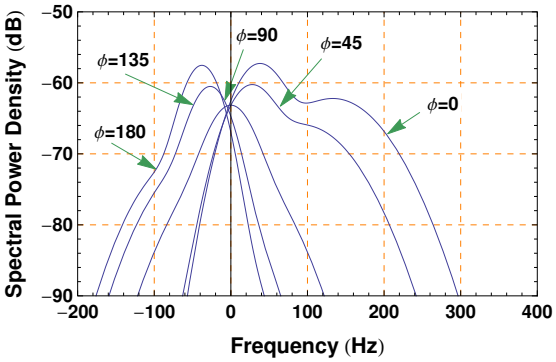

(d) sea state 3, method 2

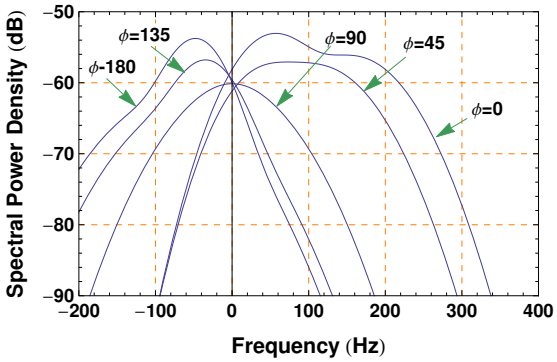

(e) sea state 5, method 1

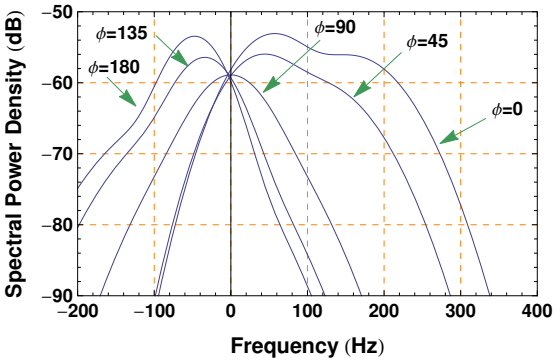

(f) sea state 5, method 2

Figure 14: *Predicted power spectral density ($m^2/m^2/Hz$), expressed in dB, of vertical polarisation sea clutter at 9300 MHz, using the modified NRL clutter model, at a grazing angle of* 2°*, for wind aspect ϕ between* 0° *and* 180°

References

1. Baker, C.J., Ward, K.D., and Watts, S., "The significance and scope of the compound K-distribution model for sea clutter", *IEE Conference Publication 281, Radar-87*, 1987, pp 207-211

2. Barton, D., *Radars, Volume 5, Radar Clutter*, Artech House, 1975

3. Branson, J., "Naval Environmental Clutter, Attenuation and Propagation Specification - NECAPS 3", DERA, July 2000

4. Farina, A., Gini, F., Greco, M.V.,and Lee, P.H.Y., "Improvement factor for real sea-clutter Doppler frequency spectra", *IEE Proceedings, Radar, Sonar & Navigation*, Vol 143, No 5, October 1996

5. Gregers-Hansen, V., and Mital, R.. "An Empirical Sea Clutter Model for Low Grazing Angles", *IEEE Radar Conference 2009*, pp 1-5

6. Horst, M.M., Dyer, F.B., and Tuley, M.T., "Radar sea clutter model", *International IEEE AP/S URSI Symposium*, Maryland, 1978, pp 6-10

7. Nathanson, F., *Radar Design Principles*, McGraw Hill New York, 1991, 2nd edition

8. Lamont-Smith, T., Ward, K.D., Walker, D.,"A comparison of EM scattering results and radar sea clutter", *IEE Radar 2002 International Conference*, pp 439-443

9. Lamont-Smith, T., "Azimuth dependence of Doppler spectra of sea clutter at low grazing angle", *IET Radar Sonar and Navigation*, vol 2, no 2, 2008, pp 97-103

10. Lee, P.H.Y., "Angle and Polarization Dependent Microwave Backscatter from Ocean Waves", *IEEE Geoscience and Remote Sensing Symposium*, IGARSS '94,1994, Vol 3, pp 1272-1274

11. Lee, P.H.Y., Barter, J.D., Beach, K.L., Hindman, C.L., Lake, B.M., Rungaldier, H., Shelton, J.C., Williams, A.B., Yee, R., and Yuen, H.C. "X band microwave backscattering from ocean waves", *Journal of Geophysical Research*, Vol 100, No C2, Feb 15, 1995, pp 2591-2611

12. Lee, P.H.Y., Barter, J.D., Beach, K.L., Caponi, E., Hindman, C.L., Lake, B.M., Rungaldier, H., and Shelton, J.C., "Power spectral lineshapes of microwave radiation backscattered from sea surfaces at small grazing angles", *IEE Proc.-Radar Sonar and Navigation*, Vol 142, No 5, October 1995, pp 252-258

13. Lee, P.H.Y, Barter, J.D., Lake, B.M., and Thompson, H.R., "Lineshape analysis of breaking-wave Doppler spectra", *IEE Proc.-Radar Sonar and Navigation*, Vol 145, No 2, April 1998, pp 135-139

14. Pidgeon, V.W., "Doppler Dependence of Radar Sea Return", *Journal of Geophysical Research*, Vol 73, No 4 Feb 15, 1968, pp 1333-1341

15. Plant, W.J., "A model for microwave Doppler sea return at high incidence angles: Bragg scattering from bounded tilted waves", *Journal of Geophysical Research*, vol 102, C9, pp 21131-21146, September 15, 1997

16. Plant, W.J., Keller, W.C. and Hayes, K., "X-band Backscatter from the Ocean at Low-Grazing Angles", *IEEE International GeoScience and Remote Sensing Symposium*, 2007

17. Plant, W.J., "A stochastic multiscale model of microwave backscatter from the ocean", *Journal of Geophysical Research*, vol 107, no C9, 2002

18. Plant, W.J., "Dual-Polarized, Coherent Microwave Backscatter From Rough Water Surfaces At Low Grazing Angles", *IEEE IGARSS 2010*, pp 4729-4732

19. Plant, W.J., Keller, W.C., Hayes, K., and Chatham, G., "Normalised radar cross section of the sea for backscatter: 1 Mean levels", *Journal of Geophysical Research*, vol 115, C09032, 2010

20. Reilly, J.P., "Clutter Models For Shipboard Radar Applications: 0.5 to 70 GHz", Technical Report, Task 3-1-18, Multisensor Propagation Data and Clutter Modelling, NATO AAW System Program Office, NAAW-88-062R, June 10, 1988

21. Reilly, J.P., and Dockery, G.D., "Influence of evaporation ducts on radar sea return", *IEE Proceedings*, Vol 137, Part F, No 2, April 1990, pp 80-88

22. Rozenberg, A.D., Quigley, D.C., and Melville, W.K., "Laboratory Study of Polarized Scattering by Surface Waves at Grazing Incidence: Part 1–Wind Waves", *IEEE Transactions on Geoscience and Remote Sensing*, Vol 33, no 4, July 1995, pp 1037-1046

23. Rozenberg, A.D., Quigley, D.C., and Melville, W.K., "Laboratory Study of Polarized Scattering by Surface Waves at Grazing Incidence: The Influence of Long Waves", *IEEE Transactions on Geoscience and Remote Sensing*, Vol 34, no 6, November 1996, pp 1331-1342

24. Skolnik, M. "Radar: Reflections and Speculations", *IEEE Radar Conference, Radar '08*, Rome, Italy, pp 1-6

25. "Radar Workstation", Technology Service Corporation

26. Walker, D.,"Doppler modelling of radar sea clutter", *IEE Proc.-Radar Sonar and Navigation*, Vol 148, No 2, April 2001

27. Walker, D.,"Experimentally motivated model for low grazing angle radar Doppler spectra of the sea surface", *IEE Proc.-Radar Sonar and Navigation*, Vol 147, No 3, June 2000

28. Ward, K.D., "A radar sea clutter model and its impact on performance assessment", *IEE Conference Radar 82*, October 1982

29. Ward, K.D., Baker, C.J., and Watts, S, "Maritime Surveillance Radar, Part 1: Radar scattering from the ocean surface." *IEE Proceedings, Part F*, Vol 137, No 2, April 1990

30. Watts, S., Ward, K., and Tough, R., "Modelling the shape parameter of sea clutter", *Radar Conference - Surveillance for a Safer World,* 2009, pp 1-6

31. "Radar Clutter", Chapter 12 of *Radar Handbook*, 3rd edition by M. Skolnik

THIS PAGE IS INTENTIONALLY BLANK

DISTRIBUTION LIST

A Model of Low Grazing Angle Sea Clutter for Coherent Radar Performance Analysis

J L Whitrow

AUSTRALIA

DEFENCE ORGANISATION	**No. of Copies**
Task Sponsor	
DGNACC, AVM K Osley	1 Printed
S&T Program	
Chief Defence Scientist Chief, Projects and Requirements Division DG Science Strategy and Policy	Doc. Data Sheet & Exec. Summary
Counsellor Defence Science, London	Doc. Data Sheet
Counsellor Defence Science, Washington	Doc. Data Sheet
Scientific Adviser Intelligence and Information	1
Navy Scientific Adviser	1
Scientific Adviser - Army	1
Air Force Scientific Adviser	1
Scientific Adviser - VCDF	Doc. Data Sheet & Dist. List
Scientific Adviser - CJOPS	Doc. Data Sheet & Dist. List
Scientific Adviser - Strategy	Doc. Data Sheet & Dist. List
Deputy Chief Defence Scientist Platform and Human Systems	Doc. Data Sheet & Exec. Summary
Chief, Electronic Warfare and Radar Division	Doc. Data Sheet & Dist. List
Dr A Shaw, RLTREP, EWRD	1
DST NACC, Dr T Priest	1
DST NACC, R Dykstra	1
S Capon, A/HAAR	1
M Dragovic, EWRD	1
T Coombs, EWRD	1
R Langdon, EWRD	1
Dr L Rosenberg	1
Dr P Berry, EWRD	1
Dr J Morris, EWRD	1
Dr J Whitrow, EWRD	1

DSTO Library and Archives	
Library Fishermans Bend	Doc. Data Sheet
Library Edinburgh	1 Printed
Library, Sydney	Doc. Data Sheet
Library Canberra	Doc. Data Sheet
Capability Development Group	
Director General Maritime Development	Doc. Data Sheet
Director NCW Development	Doc. Data Sheet
Assistant Secretary Investment Analysis	Doc. Data Sheet
RPDE Liaison Officer	Doc. Data Sheet & Exec. Summary & Dist. List
Chief Information Officer Group	
DICTF	Doc. Data Sheet
Strategy Executive	
Policy Officer, Counter–Terrorism and Domestic Security	Doc. Data Sheet
Vice Chief of the Defence Force Group	
SO (Science) – Counter Improvised Explosive Device Task Force	Doc. Data Sheet & Exec. Summary & Dist. List
Joint Logistics Command	
Directorate of Ordnance Safety Head Engineering Systems	1
Director General Strategic Logistics	Doc. Data Sheet
Military Strategic Commitments	
Director General Military Strategic Commitments	Doc. Data Sheet
Navy	
Australian Maritime Warfare Centre CAPT Peter Scott – Commander , AMWC Mr Kenneth James – Deputy Director AMWC	Doc. Data Sheet & Dist. List
Director General Navy Capability Plans & Engagement	Doc. Data Sheet
Director General Navy Communications & Information Warfare	Doc. Data Sheet
Director General Navy Certification and Safety	Doc. Data Sheet
Director General Submarine Capability Management	Doc. Data Sheet
Director General Technical Seaworthiness	Doc. Data Sheet
Australian Hydrographer	Doc. Data Sheet
Director General Logistics – Navy	Doc. Data Sheet
Head Navy Engineering	Doc. Data Sheet
Commodore Training	Doc. Data Sheet
Commander Surface Force	Doc. Data Sheet

Commander Mine Warfare, Hydrographic, and Patrol Force	Doc. Data Sheet
Commander Fleet Air Arm	Doc. Data Sheet
Commander Submarine Force	Doc. Data Sheet
Commodore War	Doc. Data Sheet
Commodore Support	Doc. Data Sheet
SO Science Fleet Headquarters	1
Army	
Australian National Coordination Officer ABCA (AS NCO ABCA), Land Warfare Development Centre, Puckapunyal	Doc. Data Sheet
SO(Science) Forces Command	1
Director Special Operations Science and Technology	Doc. Data Sheet & Exec. Summary & Dist. List
SO(Science) 1st Division	Doc. Data Sheet
SO2 S&T FDG LWDC – (Staff Officer for Science and Technology, Force Development Group)	Doc. Data Sheet
SO(Science) 1Bde	Doc. Data Sheet
SO(Science) 3Bde	Doc. Data Sheet
SO(Science) 17 CSS Bde	Doc. Data Sheet
J86 (TCS GROUP), DJFHQ	Doc. Data Sheet
Air Force	
SO (Science) – Headquarters Air Combat Group, RAAF Base, Williamtown NSW 2314	Doc. Data Sheet & Exec. Summary
Staff Officer Science Surveillance and Response Group	Doc. Data Sheet & Exec. Summary
SO (Science) Combat Support Group	Doc. Data Sheet & Exec. Summary
Staff Officer Science HQ Air Lift Group	Doc. Data Sheet & Exec. Summary & Dist. List
Intelligence and Security Group	
AS Transnational and Scientific Intelligence, DIO	Doc. Data Sheet
Manager, Information Centre, Defence Intelligence Organisation	1
Director Advanced Capabilities, DIGO	Doc. Data Sheet
Defence Materiel Organisation	
CoS GM Systems	Doc. Data Sheet
Program Manager Air Warfare Destroyer	Doc. Data Sheet
Guided Weapon & Explosive Ordnance Branch (GWEO)	Doc. Data Sheet
Director Engineering Operations; Land Engineering Agency (Michael Yates)	Doc. Data Sheet
CSIO	Doc. Data Sheet

Deputy Director Joint Fuel & Lubricants Agency	Doc. Data Sheet
Systems Engineering Manager CBRNE Program Office, Land Systems Division	Doc. Data Sheet

OTHER ORGANISATIONS

National Library of Australia	1
NASA (Canberra)	1

UNIVERSITIES AND COLLEGES

Australian Defence Force Academy

Library	1
Head of Aerospace and Mechanical Engineering	1
Hargrave Library, Monash University	Doc. Data Sheet

OUTSIDE AUSTRALIA

INTERNATIONAL DEFENCE INFORMATION CENTRES

US Defense Technical Information Center	1
UK Dstl Knowledge Services	1
Canada Defence Research Directorate R&D Knowledge & Information Management (DRDKIM)	1
NZ Defence Information Centre	1

ABSTRACTING AND INFORMATION ORGANISATIONS

Library, Chemical Abstracts Reference Service	1
Engineering Societies Library, US	1
Materials Information, Cambridge Scientific Abstracts, US	1
Documents Librarian, The Center for Research Libraries, US	1
International Technology and Science Center (ITSC) Library	1

Spare Copies	4 Printed

Total number of copies: 38 Printed: 6 PDF: 32

DEFENCE SCIENCE AND TECHNOLOGY ORGANISATION DOCUMENT CONTROL DATA				1. CAVEAT/PRIVACY MARKING
2. TITLE A Model of Low Grazing Angle Sea Clutter for Coherent Radar Performance Analysis			3. SECURITY CLASSIFICATION Document (U) Title (U) Abstract (U)	
4. AUTHOR J L Whitrow			5. CORPORATE AUTHOR Defence Science and Technology Organisation PO Box 1500 Edinburgh, South Australia 5111, Australia	
6a. DSTO NUMBER DSTO–TR–2864	6b. AR NUMBER 015-661		6c. TYPE OF REPORT Technical Report	7. DOCUMENT DATE June, 2013 Corrected March, 2017
8. FILE NUMBER 2012/1130800/1	9. TASK NUMBER AIR 07/046	10. TASK SPONSOR DGNACC	11. No. OF PAGES 35	12. No. OF REFS 31
13. URL OF ELECTRONIC VERSION `http://www.dsto.defence.gov.au/publications/scientific.php`			14. RELEASE AUTHORITY Chief, Electronic Warfare and Radar Division	

15. SECONDARY RELEASE STATEMENT OF THIS DOCUMENT

Approved for Public Release

OVERSEAS ENQUIRIES OUTSIDE STATED LIMITATIONS SHOULD BE REFERRED THROUGH DOCUMENT EXCHANGE, PO BOX 1500, EDINBURGH, SOUTH AUSTRALIA 5111

16. DELIBERATE ANNOUNCEMENT

No Limitations

17. CITATION IN OTHER DOCUMENTS

No Limitations

18. DSTO RESEARCH LIBRARY THESAURUS

sea clutter	Doppler radar
maritime surveillance	performance evaluation
radar measurement	spectral analysis

19. ABSTRACT

Pulse Doppler radar systems are increasingly being used for airborne maritime surveillance roles, but current models for sea clutter do not incorporate the spectral information required to analyse the detection performance of these systems in the low grazing angle maritime environment. This report uses standard radar sea clutter models, and spectral information from wavetank and open ocean measurements to deduce the amplitudes, Doppler frequencies, and bandwidths of the Bragg, whitecap and spike components, which together comprise the sea clutter return. This version of the report incorporates corrections listed in the Corrigenda.